Vietnam Journal of Earth Sciences, 1–32, https://doi.org/10.15625/2615-9783/25087

**Vietnam Journal of Earth Sciences**
https://vjs.ac.vn/index.php/jse

# Chromophoric and fluorescent dissolved organic matter in the Red River (Northern Vietnam): Hydrological-period contrasts and spatial variability

Thi Quynh Mai Duong[1,2], Nguyen Hoang Anh Chu[3], Van Hoi Bui[1], Huong Mai[1], Catherine Guigue[1,2], Marc Tedetti[1,2], Vincent Grossi[2], Cam Tu Vu[1*]

[1]*University of Science and Technology of Hanoi (USTH), VAST, Hanoi, Vietnam*
[2]*Aix Marseille Univ, Université de Toulon, CNRS, IRD, MIO, Marseille, France*
[3]*Institute of Ecology, Tallinn University, Narva mnt 25, 10120 Tallinn, Estonia*

Received 04 April 2026; Received in revised form 11 June 2026; Accepted 17 August 2026

ABSTRACT

Dissolved organic matter (DOM) dynamics in large tropical rivers play a key role in aquatic carbon cycling, yet remain poorly documented in Vietnamese systems, particularly for chromophoric and fluorescent DOM (CDOM and FDOM). In this study, 68 surface water samples were collected along the main channel of the Red River (northern Vietnam), from upstream regions to the estuary, during the dry (March) and wet (July) periods of 2019. CDOM and FDOM characteristics were investigated using UV-visible absorbance and excitation-emission matrix (EEM) fluorescence spectroscopy coupled with parallel factor analysis (PARAFAC). A three-component PARAFAC model identified two humic-like components (C1 and C3) and one tryptophan-like component (C2). Significant differences between the two sampling periods, representing contrasting hydrological conditions, and marked spatial variability were observed. CDOM and FDOM concentrations were significantly higher during the wet period, with CDOM absorption coefficient at 350 nm [a(350)] of 4.8±2.2 $m^{-1}$ (wet) and 1.9±0.8 $m^{-1}$ (dry), specific ultraviolet absorbance ($SUVA_{254}$) of 10.0±2.6 L mg $C^{-1}$ $m^{-1}$ (wet) and 4.3±0.8 L mg $C^{-1}$ $m^{-1}$ (dry), C1 of 118±25 QSU (wet) and 66±29 QSU (dry), C3 of 74±10 QSU (wet) and 47±23 QSU (dry), and C2 of 418±85 QSU (wet) and 119±63 QSU (dry). These patterns reflected enhanced terrestrial inputs driven by monsoon runoff and soil leaching, resulting in more aromatic, higher-molecular-weight DOM. Along the river continuum, upstream waters were dominated by humic, terrestrially derived material (higher values of DOC, a(350), C1, C3). In contrast, the Red River Delta exhibited lower DOM concentrations and greater material processing, consistent with dilution and in-river processing. The higher relative contribution of tryptophan-like compounds (higher %C2, C2/C1, and C2/C3 ratios) in the delta during the dry period may reflect enhanced biological activity and/or possible anthropogenic inputs. These findings highlight the combined influence of monsoon hydrology, in-stream processes, and human pressures on DOM dynamics in a major Southeast Asian river.

*Keywords:* Red River, Vietnam, Dissolved organic matter, CDOM, FDOM, EEM-PARAFAC.

## 1. Introduction

Characterizing dissolved organic matter (DOM) is essential for understanding biogeochemical processes and water quality in river systems (Leenheer and Croué, 2003; Zhang et al., 2021). The Red River (Northern Vietnam), one of the largest river systems in Southeast Asia, drains diverse landscapes including forested catchments, agricultural

*Corresponding author, Email: vu-cam.tu@usth.edu.vn

lands, and densely urbanized zones (Le et al., 2017; Luu et al., 2012; Yuen et al., 2021). This environmental heterogeneity generates a complex mixture of DOM sources, ranging from allochthonous inputs derived from soil and vegetation to autochthonous production from microbial and algal activity. In addition, monsoon-driven hydrological variability strongly modulates the mobilization, transport, and transformation of organic matter (Jaffé et al., 2013; Yamashita et al., 2010). In this system, DOM plays a central role in carbon cycling, nutrient transport, photochemical reactivity, and contaminant dynamics (Le et al., 2017).

The Red River exports substantial amounts of organic carbon from terrestrial ecosystems to coastal waters (Nguyen et al., 2021; 2022; Piton et al., 2020; Wei et al., 2019). Between 2003 and 2013, dissolved organic carbon (DOC) and particulate organic carbon (POC) fluxes at the Red River outlet reached 222 and 406 kt $yr^{-1}$, respectively, with nearly 80% occurring during the rainy season. Together, these fluxes accounted for about 0.38% of the total organic carbon (TOC) exported by Asian rivers to the ocean (Fabre et al., 2023; Le et al., 2017). These findings highlight the importance of hydrological seasonality in regulating carbon export and underscore the need to characterize better the composition and sources of DOM transported by the river. Despite its regional significance, detailed investigations of DOM composition, sources and transformation processes in the Red River remain limited, particularly using advanced spectroscopic approaches.

The optically active components of the DOM, known as chromophoric DOM (CDOM), i.e., the fraction of the DOM which absorbs radiation over the ultraviolet (UV; 200–400 nm) and visible (Vis; 400–700 nm) spectral domains (Bricaud et al., 1981), and fluorescent DOM (FDOM), i.e., the fraction of the CDOM which emits fluorescence after absorbing UV-Vis radiation (Duursma, 1974), have been extensively investigated (separately or together) for several decades to understand and assess the sources, composition/quality, distribution and reactivity/fate of DOM in natural waters (Fellman et al., 2010; Hudson et al., 2007; Stedmon and Cory, 2014). Focusing on CDOM and FDOM has been motivated by several factors. First, they represent significant fractions of DOM, with CDOM accounting for approximately 20% of DOC in the open ocean and up to 70% in coastal waters (Coble, 2007; Laane and Koole, 1982). Second CDOM and FDOM can be rapidly characterized by UV-Vis absorbance and fluorescence spectroscopy using small water volumes and minimal sample preparation, whereas DOM remains one of the most complex molecular mixtures known on Earth (Dittmar et al., 2021; Dittmar and Stubbins, 2014). In addition, CDOM and FDOM strongly influence underwater light attenuation, ocean color, photochemical reactions, and interactions with contaminants, thereby affecting aquatic biogeochemical cycles and ecosystem functioning (Coble, 2007; Nelson and Siegel, 2013; Tedetti et al., 2026).

CDOM and FDOM parameters provide quantitative proxies for DOM structural characteristics, such as aromaticity, apparent molecular weight, and humification degree (D'Andrilli et al., 2022; Helms et al., 2008; Korak and McKay, 2024; Li and Hur, 2017). Fluorescence excitation-emission matrix (EEM) spectroscopy coupled with parallel factor analysis (PARAFAC) allows for the identification of distinct fluorescent components within FDOM, typically categorized as protein- and humic-like substances (Coble, 1996; Stedmon et al., 2003; Stedmon and Bro, 2008). These components serve as markers for terrestrial inputs, autochthonous biological production, microbial degradation, abiotic photobleaching, or anthropogenic inputs. The use of optical approaches and the

determination of CDOM and FDOM parameters in other Asian river systems has proven to be very relevant for tracking spatio-temporal variations in DOM associated with land use, hydrology, and climatic variability (Jaffé et al., 2014; Kang et al., 2023; Mielnik and Kowalczuk, 2018; Shi et al., 2020). However, very little data currently exists on CDOM and FDOM in the Red River (Martinot et al., 2025).

In this context, this study aims to characterize CDOM and FDOM and investigate their variability across contrasting hydrological conditions and along the Red River continuum, from upstream reaches to the estuary, during dry- and wet-period sampling campaigns conducted in March and July 2019. By combining optical indices with multicomponent fluorescence modeling, this work provides new insights into DOM sources, transformations, and hydrological controls in a tropical monsoon-influenced river system, contributing to a more comprehensive understanding of carbon cycling in Northern Vietnam.

## 2. Materials and Methods

### *2.1. Study area*

The Red River system is one of the largest and most important river systems in Southeast Asia. It originates in Yunnan Province (China). It flows through Northern Vietnam before discharging into the Gulf of Tonkin (East Sea of Vietnam) in large part *via* the Ba Lat estuary (Fig. 1). The river extends approximately 1,149 km, including ~510 km within Vietnam. It drains a basin of ~169,000 km$^2$, more than half of which lies in Vietnamese territory. In Northern Vietnam, the Red River crosses diverse landscapes, including mountainous forested catchments in the upstream region (UpR), agricultural plains, and densely populated urban centers such as Hanoi, the capital city. Downstream, it forms the Red River Delta (RRD), one of Vietnam's most fertile and densely populated regions, characterized by intensive rice cultivation and aquaculture. The Red River flows into the Gulf of Tonkin through nine river mouths, of which Ba Lat is the main channel (Nguyen et al., 2025) (Fig. 1).

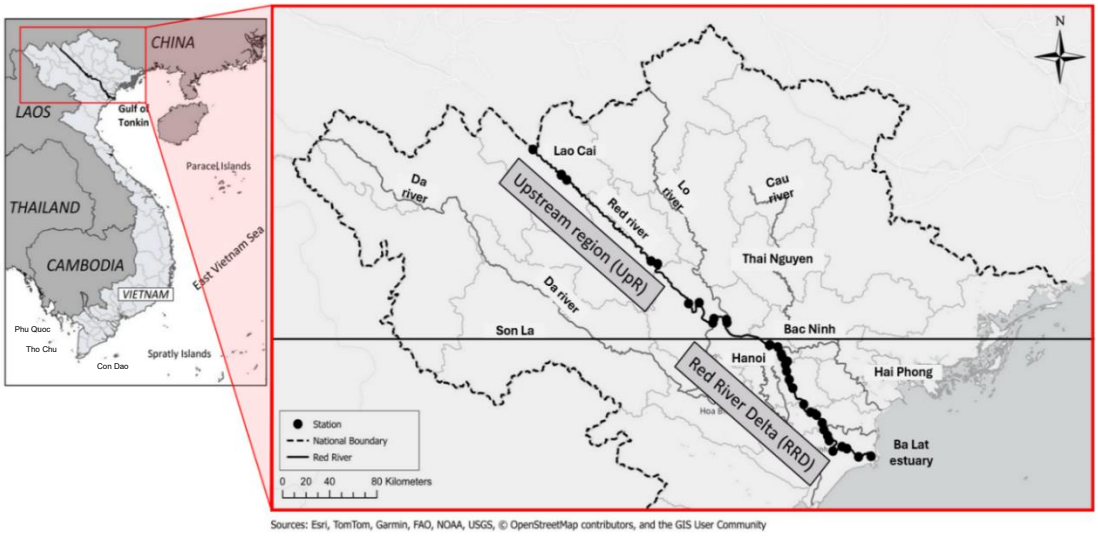


*Figure 1.* Study area and location of the 34 sampling stations investigated in March and July 2019 along the main channel of the Red River, from the upstream region (UpR) to the Red River Delta (RRD) and the Ba Lat estuary (Northern Vietnam)

Along this gradient, population density rises from < 300 inhabitants $km^{-2}$ in the UpR to > 1000 inhabitants $km^{-2}$ in the RRD (Le et al., 2020). Upstream soils are mainly red and yellow-brown earth. In contrast, the delta consists of tidally influenced alluvial soils ranging from sandy near river channels to silty and clay-rich further inland (Huong et al., 2013). Land use shifts from predominantly forest (74%) and agriculture (19%) in the UpR to intensive agriculture in the RRD, where ~80% of the population is engaged in farming. The delta is Vietnam's second-largest rice-producing region (~20% of national production), with rice, vegetables, grains, peanuts, fruits, tea, medicinal plants, and poultry as major products (Huong et al., 2013; Le et al., 2015; Redfern et al., 2012).

The Red River basin is characterized by a humid tropical monsoon climate with two distinct seasons: a hot, wet season (May-October) driven by the summer monsoon, and a cooler, dry season (November-April) associated with the winter monsoon (Le et al., 2007; Vinh et al., 2014; Xue et al., 2016). The wet season accounts for approximately 85% of the annual precipitation (with average annual precipitation ranging from 800 to 3000 mm; Nguyen et al., 2025) and largely controls river discharge, sediment transport, and DOM dynamics, with most annual water and organic carbon fluxes occurring during this period due to intense rainfall and runoff.

### *2.2. Sampling, in situ measurements and filtration*

Surface water was collected at 34 stations (St 1-34) along the main channel of the Red River (Fig. 1), spanning from the UpR through the mountain areas (from Lao Cai to Phu Tho province, 10 stations, St 1-10) to the RRD region (from Hanoi to the Ba Lat estuary, 24 stations, St 11-34). Sampling was conducted during the dry period (1-7 March 2019) and the wet period (1-10 July 2019). Stations were selected based on topography and the intensity of human activities along the riverbanks, using field surveys and national land-use statistics (CEIC Data, Vietnam, https://www.ceicdata.com), to assess the influence of land use and anthropogenic pressures on DOM characteristics (Vu et al., 2023). Agricultural and forestry inputs were targeted at St 4 and St 6, whereas urban and industrial non-point sources were monitored at St 1-2, St 5, St 7-12, St 22, and St 28. Point-source domestic and industrial discharges were sampled at St 3, St 13-21, and St 24-25. Downstream stations (St 23 and St 26-33) were located near intensive agricultural areas, and the Ba Lat estuarine end-member was collected at St 34 in Ninh Binh. Geographic coordinates and station characteristics are provided in Table 1.

At each station, surface water was collected at approximately 50-cm depth using 500-mL acid-washed high-density polypropylene (HDPP) bottles (SPL, Korea). HDPP bottles were pre-washed with 1 M hydrochloric acid (HCl) and ultrapure water (Milli-Q, 18.2 MΩ cm), and rinsed thoroughly with the river sample before filling. Samples were stored in cool, dark conditions (~4°C) during field sampling and transport to the laboratory. Concomitantly with water sampling, *in situ* physico-chemical parameters, including water temperature, electrical conductivity (EC), pH and dissolved oxygen (DO), were measured using a portable multiparameter probe (HI98196, Hanna Instruments, USA).

Upon return, water samples were filtered through pre-combusted (500°C, 6 h) glass fiber filters (GF/F, Whatman, ~0.7 µm pore size). Before filtration, filters were rinsed with ultrapure water, and a small volume of sample (~20 mL) was used. Filtered water samples were transferred into 20-mL pre-combusted glass tubes for CDOM, FDOM, and DOC analyses, and into 50-mL HDPP bottles for nutrient analyses. DOC samples were acidified with 50 µL of concentrated HCl (37%, Merck). The samples were then kept in the dark at 4°C before analysis.

*Table 1.* Sampling stations along the Red River, with corresponding city/province, coordinates, and main types of land usage

| Region | Station | City/province | Coordinates (°N, °E) | | Land use |
|---|---|---|---|---|---|
| Upstream (UpR) | St 1 | Lao Cai | 22.499856 | 103.969713 | UrRA*, ForL |
| | St 2 | Lao Cai | 22.319155 | 104.187570 | UrRA*, ForL |
| | St 3 | Lao Cai | 22.316016 | 104.184653 | SubUrRA*, ForL |
| | St 4 | Lao Cai | 22.280715 | 104.227462 | ForL, AgriF |
| | St 5 | Lao Cai | 21.697087 | 104.869971 | URA*,FarL, AgriF |
| | St 6 | Lao Cai | 21.677326 | 104.919976 | RuRA**, ForL, FarL |
| | St 7 | Phu Tho | 21.391593 | 105.156208 | RuRA**, FarL, AgriF |
| | St 8 | Phu Tho | 21.397302 | 105.236965 | RuRA**, FarL, AgriF |
| | St 9 | Phu Tho | 21.252388 | 105.341111 | RuRA*, FarL and AgriF |
| | St 10 | Phu Tho | 21.283111 | 105.349194 | RuRA*, AgriF, Sand-MF |
| Red River Delta (RRD) | St 11 | Hanoi | 21.276000 | 105.445000 | SubUrRA*, AgriF, IndusF |
| | St 12 | Hanoi | 21.254388 | 105.448500 | SubUrRA*, AgriF, Sand-MF |
| | St 13 | Hanoi | 21.092611 | 105.771805 | URA*, AgriF, IndusF |
| | St 14 | Hanoi | 21.094388 | 105.775388 | URA*, IndusF, Sand-MF |
| | St 15 | Hanoi | 21.079000 | 105.836694 | URA**, FarL, AgriF |
| | St 16 | Hanoi | 21.029178 | 105.862164 | URA*, FarL |
| | St 17 | Hanoi | 21.007416 | 105.869888 | URA*, AgriF |
| | St 18 | Hanoi | 20.975483 | 105.909271 | SubUrRA*, AgriF |
| | St 19 | Hanoi | 20.953167 | 105.893973 | SubUrRA**, AgriF, IndusF, Sand-MF |
| | St 20 | Hanoi | 20.905498 | 105.902848 | SubUrRA**, AgriF, IndusF |
| | St 21 | Hung Yen | 20.844525 | 105.922982 | RuRA**, FarL, Sand-MF |
| | St 22 | Hung Yen | 20.782966 | 105.950261 | RuRA**, FarL, IndusF |
| | St 23 | Ninh Binh | 20.666768 | 106.033057 | AgriF*, Sand-MF |
| | St 24 | Ninh Binh | 20.610009 | 106.085164 | RuRA**, AgriF, Sand-MF |
| | St 25 | Ninh Binh | 20.589432 | 106.131255 | RuRA*, AgriF, Sand-MF |
| | St 26 | Ninh Binh | 20.533491 | 106.174165 | RuRA**, AgriF |
| | St 27 | Ninh Binh | 20.484654 | 106.186665 | RuRA*, AgriF, IndusF |
| | St 28 | Ninh Binh | 20.440940 | 106.214951 | SubUrRA*, AgriF |
| | St 29 | Ninh Binh | 20.405837 | 106.227779 | UrRA* |
| | St 30 | Ninh Binh | 20.330721 | 106.256189 | RuRA**, AgriF |
| | St 31 | Ninh Binh | 20.362017 | 106.325080 | AgriF, Sand-MF |
| | St 32 | Ninh Binh | 20.347919 | 106.362737 | RuRA**, AgriF |
| | St 33 | Ninh Binh | 20.288813 | 106.451244 | AgriF, Sand-MF |
| | St 34 | Ninh Binh | 20.293157 | 106.546080 | RuRA**, AgriF, Sand-MF, Estuary |

*High population density > 1000 inhabitants $km^{-2}$; ** Low population density < 1000 inhabitants $km^{-2}$; UrRA: Urban residential area; SubUrRA: Suburban residential area; RuRA: Rural residential area; ForL: Forest land; FarL: Farm land for growing fruits, perennial plants; AgriF: Agricultural field for growing vegetables, rice, grain, peanut, tea, flowers, etc.; IndusF: Industrial field; Sand-MF: Sand mining field

### *2.3. Analyses and data treatment*

#### *2.3.1. Nutrients*

Ammonium ($NH_4^+$), nitrate ($NO_3^-$), and phosphate ($PO_4^{3-}$) concentrations were determined by UV spectrophotometry using a UV-1800 spectrophotometer (Shimadzu) following Vu et al. (2023). Calibration curves were established using standard solutions prepared in ultrapure water, and procedural

blanks and replicate analyses were regularly performed to ensure analytical quality and precision.

*2.3.2. Dissolved organic carbon (DOC)*

Acidified water samples for DOC determination were analyzed using the non-purgeable organic carbon (NPOC) method with a Shimadzu TOC-V CPN Total Organic Carbon Analyzer (Kyoto, Japan), based on high-temperature catalytic oxidation over platinum followed by non-dispersive infrared detection of $CO_2$ (Fourrier et al., 2022; Sohrin and Sempéré, 2005). Calibration was performed using potassium hydrogen phthalate standard solutions prepared in ultrapure water. Instrumental performance and system blanks were validated using certified reference materials (Batch 11, Lot # 06-11, Hansell Laboratory), with analytical precision better than 2%.

*2.3.3. Chromophoric dissolved organic matter (CDOM)*

Samples were thawed and brought to room temperature (20°C) in the dark, then transferred into a 1-cm Suprasil quartz cuvette for absorbance measurements in single-beam mode using a Shimadzu UV-Vis 1800 spectrophotometer, according to Ferretto et al. (2017) and Martinot et al. (2025). CDOM absorbance spectra were generated from 200 to 800 nm with 1 nm intervals, a slit width of 1 nm, and a scan speed of 230 nm $min^{-1}$. Ultrapure water blanks were analyzed daily together with the sample series. Replicating analyses of the same samples yielded absorbance measurements with better than 3% precision over the 220–700 nm range.

The absorbance spectra of samples were corrected for blank (mean absorbance spectrum of ultrapure water) and baseline drift (by subtracting, for each sample, the mean absorbance value between 650 and 700 nm from the whole absorbance spectrum). CDOM absorption coefficients [a(λ) in $m^{-1}$] were then calculated from the corrected absorbance spectra (Andrew et al., 2013; Yamashita et al., 2013) from the following equation:

$$a(\lambda) = \frac{A(\lambda) \times 2.303}{L}$$

where A(λ) is the absorbance value at wavelength λ (unitless), L is the path length (0.01 m) of the quartz cuvette, 2.303 is the factor allowing the conversion of the A(λ) value from base 10 log into neperian base log, and a(λ) is the CDOM absorption coefficient at wavelength λ ($m^{-1}$). Here, we report CDOM absorption coefficients at 254 and 350 nm [a(254) and a(350)], commonly used as proxies for CDOM abundance.

CDOM spectral slope coefficients were determined from 275 to 295 nm ($S_{275-295}$ in $nm^{-1}$) and from 350 to 400 nm ($S_{350-400}$ in $nm^{-1}$) as the proxies of DOM average molecular weight (Helms et al., 2008), by applying a nonlinear (exponential) regression to the values of a(λ), in accordance with the following formula (Bricaud et al., 1981; Nelson et al., 2007):

$$a(\lambda) = a(\lambda_0) \times e^{-S(\lambda - \lambda_0)}$$

where a(λ) and $a(\lambda_0)$ are respectively the CDOM absorption coefficients ($m^{-1}$) at wavelengths λ and $\lambda_0$ (with $\lambda_0 < \lambda$, in nm), and S is the spectral slope coefficient between $\lambda_0$ and λ (in $nm^{-1}$). The regression was performed on the raw data (i.e., not log-transformed) according to the recommendations of Twardowski et al. (2004). The CDOM slope ratio ($S_R$, unitless) was calculated as the ratio of $S_{275-295}$ to $S_{350-400}$, as it is indicative of DOM molecular weight and photodegradation-induced changes in molecular weight (Helms et al., 2008).

Specific ultraviolet absorbance at 254 nm ($SUVA_{254}$, in L mg $C^{-1}$ $m^{-1}$), an indicator of DOM aromaticity, was calculated by dividing a(254) by the DOC concentration (in mg C $L^{-1}$) (Weishaar et al., 2003). The $E_2/E_3$ ratio (unitless), a proxy for DOM aromaticity and average molecular weight,

was calculated as a(250)/a(365) (De Haan and De Boer, 1987; Peuravuori and Pihlaja, 1997).

*2.3.4. Fluorescent dissolved organic matter (FDOM)*

FDOM measurements were conducted with a Horiba FluoroMax-4 spectrofluorometer with a 1-cm Suprasil quartz cuvette. EEMs were generated in signal/reference mode with instrument-corrected excitation and emission spectra, over an excitation wavelength ($\lambda_{Ex}$) range of 200–550 nm (5-nm step) and an emission wavelength ($\lambda_{Em}$) range of 280–600 nm (2-nm step), using 5-nm slit widths (Martinot et al., 2025). The sample compartment in the cell holder was thermostated at 20°C, controlled by the Newport temperature controller model 300B (Japan). Before each series of measurements, ultrapure water EEMs (blanks) were recorded, monitoring the Raman scattering peak at $\lambda_{Ex}/\lambda_{Em}$ of 275/303 nm. In addition, solutions of quinine sulfate dihydrate (1–50 μg $L^{-1}$; Fluka, purum for fluorescence) in 0.05 M sulfuric acid ($H_2SO_4$, 98%) were run at $\lambda_{Ex}/\lambda_{Em}$ of 350/450 nm (5-nm slit widths). Several post-processing steps were undertaken to correct the sample EEMs: (1) correction for the inner filter effect using absorbance data and formula by Ohno (2002), (2) correction for the blank using the mean EEM of ultrapure water, and (3) conversion into quinine sulfate unit (QSU), where 1 QSU corresponded to the fluorescence of 1 μg $L^{-1}$ quinine sulfate at $\lambda_{Ex}/\lambda_{Em}$ of 350/450 nm (Murphy et al., 2008; Tedetti et al., 2026).

PARAFAC was performed on a total of 68 sample EEMs using the DOMFluor toolbox v1.6 (Stedmon and Bro, 2008) running under MATLAB® 9.13.0 (R2022b). The EEM wavelength ranges used were 240–500 and 300–550 nm for Ex and Em, respectively. EEMs were merged into a three-dimensional data array of the form: 62 samples × 53 $\lambda_{Ex}$ × 126 $\lambda_{Em}$. One sample (St 2, dry period) was identified as an outlier and removed from the dataset. The validation of the PARAFAC model (running with the non-negativity constraint) and the determination of the correct number of components (from 2 to 5 components tested) were achieved through the examination of the percentage of explained variance, the shape of residuals, the split-half analysis, and the random initialization using the Tucker Congruence Coefficients (TCC) (Tedetti et al., 2012, 2026).

Fluorescence indices, including the fluorescence index (FI), humification index (HIX), and biological index (BIX), were calculated to evaluate DOM sources and composition better. FI (unitless), used to distinguish between microbially derived and terrestrially derived fulvic acids, was calculated as the ratio of fluorescence intensity at $\lambda_{Em}$ of 450 nm to that at $\lambda_{Em}$ of 500 nm, with $\lambda_{Ex}$ of 370 nm (McKnight et al., 2001). HIX (unitless), an indicator of the degree of humification of the DOM, was computed as the integral of the fluorescence intensities between $\lambda_{Em}$ of 435 and 480 nm divided by the integral of the fluorescence intensities between $\lambda_{Em}$ of 300 and 345 nm at $\lambda_{Ex}$ of 255 nm (Ohno, 2002). BIX (unitless), an indicator of freshly produced autochthonous DOM, was calculated as the fluorescence intensity at $\lambda_{Em}$ of 380 nm divided by the fluorescence intensity at $\lambda_{Em}$ of 430 nm at $\lambda_{Ex}$ of 310 nm (Huguet et al., 2009).

### *2.4. Statistical analyses*

Before statistical analyses, the distribution of each variable was evaluated using Shapiro-Wilk, Anderson-Darling, Lilliefors, and Jarque-Bera normality tests. Because most variables did not satisfy normality assumptions, differences between groups were assessed using the non-parametric Mann-Whitney rank-sum test (U-test). Effect sizes were calculated and reported alongside p-values. Box-and-whisker plots were used to

examine the distributions of variables by hydrological period (wet *vs*. dry) and spatial sector. Pairwise relationships among variables were explored using Pearson correlation coefficients. Comparison with Spearman rank correlations (not shown) yielded highly similar correlation patterns and overall interpretations.

Principal Component Analysis (PCA) was performed using the Pearson correlation matrix, while Ascending Hierarchical Classification (AHC) was conducted using Ward's method based on squared Euclidean distances. For both PCA and AHC, data were centered and standardized before analysis. PCA and AHC were used as exploratory multivariate techniques to identify dominant patterns and relationships among variables.

For the study of spatial variability, sampling stations were grouped into two broad spatial sectors: UpR and RRD. This classification was designed to investigate large-scale longitudinal (upstream-downstream) gradients in DOM characteristics across the river continuum rather than local-scale heterogeneity within the deltaic system. St 34, located near the Ba Lat estuary, was retained in the statistical analyses because it represents the downstream end-member of the river continuum investigated in this study. All statistical analyses were performed using XLSTAT 2024.4v.1.

### *2.5. River discharge and precipitation data*

River discharge data of the Red River were obtained from the hydrological observation station at Son Tay, provided by the Institute of Oceanography - Hai Phong Branch, Vietnam Academy of Science and Technology. The Son Tay station is located in the lower section of the Red River, upstream of the delta distributary system. It is commonly considered representative of the main freshwater discharge delivered from the Red River toward the delta and adjacent coastal waters. This station provided discharge data at daily resolution covering the sampling periods. Precipitation data for the sampling periods and for the different provinces crossed during the surveys were obtained from https://en.climate-data.org/.

## 3. Results and Discussion

### *3.1. Identification of the FDOM components validated by PARAFAC modeling*

A three-component PARAFAC model was identified as the most appropriate to describe the FDOM composition and variability in the Red River. The model's robustness was confirmed through split-half validation (four successful split-half analyses), and a high percentage of variance explained (99.6%), indicating that the extracted components were statistically reliable and reproducible. Contour plots and spectral characteristics for the three FDOM components (C1-C3), including $\lambda_{Ex}$ and $\lambda_{Em}$ maxima, are presented in Fig. 2 and Table 2. All components showed strong matches (TCC $\lambda_{Ex} \times \lambda_{Em} > 0.95$) with OpenFluor database components (Murphy et al., 2014), suggesting that the identified fluorophores are consistent with previously reported FDOM signatures in natural waters.

The first component (C1) exhibited excitation-emission maxima at $\lambda_{Ex1}$, $\lambda_{Ex2}/\lambda_{Em}$ of < 240, 340/524 nm (Fig. 2; Table 2). This component corresponds to a humic-like UV-C + UV-A fluorophore, displaying excitation peaks in both the UV-C and UV-A spectral domains, and commonly referred to as peaks A + $C^+$ (Coble et al., 2014) or peaks α' + α (Parlanti et al., 2000). It has been widely reported in freshwater and coastal environments and is generally attributed to terrestrially derived DOM originating from soil organic matter and plant material. It is typically associated with highly aromatic, humified, and high-molecular-weight compounds (Ishii and Boyer, 2012; Lin and Guo, 2020; Obrador et al., 2018; Yamashita et al., 2010) (Table 2).

The second component (C2), with $\lambda_{Ex}/\lambda_{Em}$ of 270/348 nm (Fig. 2; Table 2), is characteristic of tryptophan-like fluorescence and labeled as peak T (Coble et al., 2014) or peak δ (Parlanti et al., 2000). It is typically associated with protein-like substances derived from microbial activity, phytoplankton production, or wastewater inputs, and is often considered an indicator of recently produced or biologically labile DOM (Lee et al., 2018; Retelletti Brogi et al., 2020; Stedmon and Markager, 2005; Yan et al., 2023) (Table 2).

The third component (C3) showed excitation-emission maxima at $\lambda_{Ex1}$, $\lambda_{Ex2}/\lambda_{Em}$ of 240, 310/440 nm (Fig. 2; Table 2). This component corresponds to a humic-like UV-C + UV-B fluorophore with excitation peaks in both spectral domains. It is commonly reported as peaks A + M/C or peaks α' + β/α in the literature (Coble et al., 2014; Parlanti et al., 2000). Such components are generally attributed to relatively low-molecular-weight humic substances and may originate from both terrestrial inputs and microbial transformations within aquatic systems (Hosen et al., 2021; Ishii and Boyer, 2012; Lin and Guo, 2020; Zhuang et al., 2021) (Table 2).

Overall, the spectral characteristics and excitation-emission maxima of the three identified components are consistent with previously reported PARAFAC models of riverine DOM (Table 2), confirming the presence of a mixture of terrestrial humic substances and biologically derived protein-like material in the Red River system.

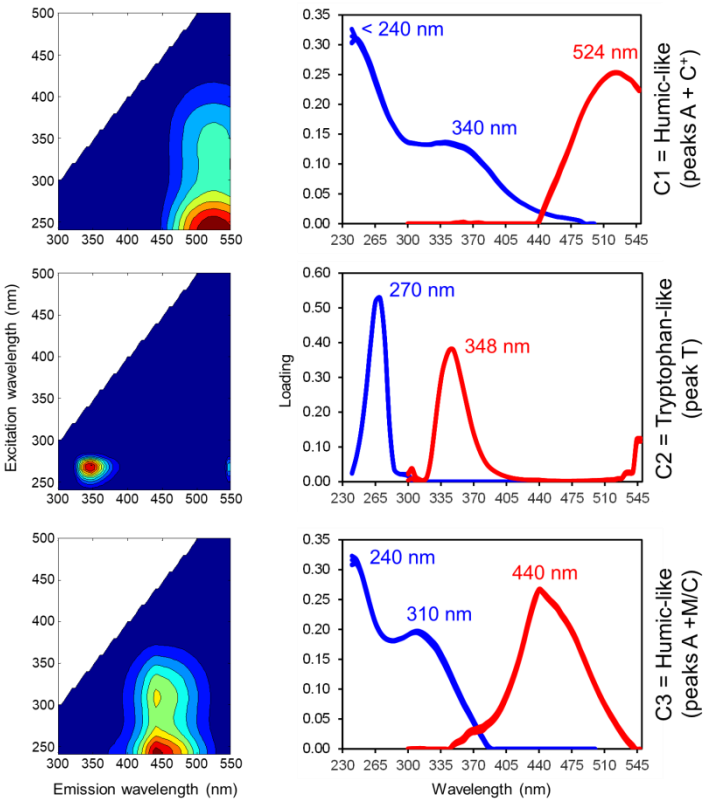


*Figure 2.* Excitation-emission fluorescence characteristics of the three PARAFAC-FDOM components identified in Red River samples: C1 (humic-like), C2 (tryptophan-like), and C3 (humic-like). Contour plots (left) and excitation/emission spectra with split-half validation results (right) are shown

*Table 2.* Excitation and emission maxima ($\lambda_{Ex}$ and $\lambda_{Em}$) of the three PARAFAC-FDOM components (C1-C3) validated for Red River samples, together with their classification (type/nature, label/name) and possible origins based on comparisons with previously reported components in the literature

| Components (this study) | $\lambda_{Ex1}$, $\lambda_{Ex2}$ / $\lambda_{Em}$ (nm) | Type/nature | Label/name | Possible origins | References |
|---|---|---|---|---|---|
| C1 | < 240, 340 / 524 | Humic-like UV-C + UV-A | Peaks A + C[+1,2]<br>Peaks α' + α[3]<br>C2[4], C2[5], C2[6], C3[7], C2[8], C4[9] | Terrestrial (soil, higher plants), terrestrial reduced quinone-like, humic acid and fulvic acid extracted from soil/sediment, autochthonous (microbial activity) | [1]Coble (2007)<br>[2]Coble et al. (2014)<br>[3]Parlanti et al. (2000)<br>[4]Ishii and Boyer (2012)<br>[5]Yamashita et al. (2010)<br>[6]Lambert et al. (2016)<br>[7]Obrador et al. (2018)<br>[8]Lin and Guo (2020)<br>[9]Osburn et al. (2016)<br>[10]Stedmon and Markager (2005)<br>[11]Ferretto et al. (2017)<br>[12]Park et al. (2021)<br>[13]Yan et al. (2023)<br>[14]Lee et al. (2018)<br>[15]Retelletti Brogi et al. (2020)<br>[16]Hosen et al. (2021)<br>[17]Zhuang et al. (2021) |
| C2 | 270 / 348 | Tryptophan-like, Protein-like | Peak T[1,2]<br>Peak δ[3]<br>C7[10], C2[11], C2[12], C2[13], C3[14], C4[15] | Autochthonous (phytoplankton, heterotrophic prokaryotes), anthropogenic (waste waters) | |
| C3 | 240, 310 / 440 | Humic-like UV-C + UV-B | Peaks A + M/C[1,2]<br>Peaks α' + β/α[3]<br>C3[4], C1[5], C1[7], C1[8], C1[16], C1[17] | Terrestrial (soil, higher plants) autochthonous (microbial activity), anthropogenic | |

### *3.2. Variability of CDOM and FDOM across contrasting hydrological periods*

The complete dataset for meteorological, hydrological, physico-chemical parameters, nutrients, DOC, CDOM, and FDOM is provided in Tables S1 and S2. Hydrological-period variability in these parameters was examined using multivariate analysis and box-and-whisker plots. PCA performed on DOC, CDOM, and FDOM parameters clearly separated samples into two groups corresponding to the dry and wet periods (Fig. 3; Table S3), a pattern also confirmed by AHC (Fig. S1). This separation mainly occurred along the first factorial axis (F1), which explained 50% of the total variance. F1 was positively associated with a(254), a(350), $SUVA_{254}$, C1, C2, and C3, and negatively associated with $E_2/E_3$ and $S_{275-295}$, whereas F2 was mainly positively associated with DOC and HIX (Fig. 3). Correlations between these parameters are reported in Table S4.

Differences between the dry and wet periods were further illustrated using box-and-whisker plots (Fig. 4)s. Water temperature (dry: 18.4±1.5°C; wet: 27.9±1.2°C), precipitation (dry: 1.4± 1.0 mm; wet: 7.6± 3.8 mm) and river discharge (dry: 1397± 196 $m^3$ $s^{-1}$; wet: 2803±270 $m^3$ $s^{-1}$) were significantly higher during the wet period (U-test, $p < 0.0001$) (Fig. 4a-c; Table S5), reflecting the influence of the monsoon-driven hydrological regime of the Red River basin (Le et al., 2007; Nguyen and Tran, 2023; Vinh et al., 2014). In contrast, EC tended to be higher and more variable during the dry period (469±1009 µS $cm^{-1}$ *vs.* 242±52 µS $cm^{-1}$; U-test, $p = 1.0$) (Fig. 4d; Table S5), likely pointing to reduced freshwater dilution and an influence of marine/saline waters toward the Ba Lat estuary. No significant hydrological-period differences were observed for $NO_3^-$, $PO_4^{3-}$ or $NH_4^+$ concentrations (U-test, $p = 0.050–0.966$) (Tables S1 and S5; Fig. 4e).

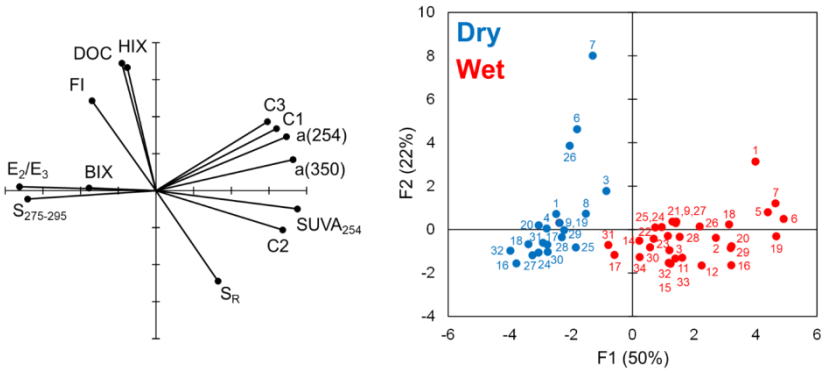


*Figure 3.* Principal component analysis (PCA) of DOC, CDOM, and FDOM parameters (n = 51). Projection of variables (left) and samples (right) on the first factorial plane (F1-F2). Dry-period (blue) and wet-period (red) samples are highlighted. Variable loadings and explained variance are provided in Table S3

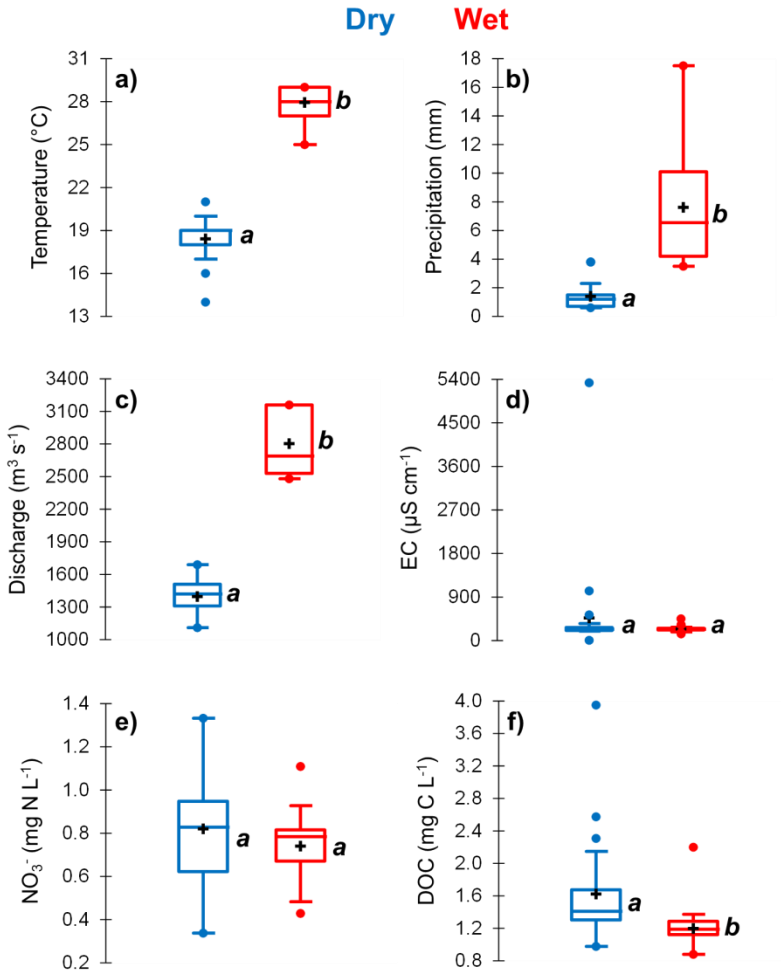


*Figure 4.* Distribution of water temperature, precipitation, river discharge, electrical conductivity (EC), nitrate ($NO_3^-$), and dissolved organic carbon (DOC) according to hydrological period: dry (blue) and wet (red). Different letters indicate significant differences between periods (U-test, $p < 0.05$; Table S5)

Interestingly, DOC concentration was significantly higher during the dry period (1.62±0.63 mg C $L^{-1}$) than during the wet period (1.20±0.23 mg C $L^{-1}$) (U-test, $p < 0.0001$) (Fig. 4f; Table S5). Previous studies on DOC in the Red River have reported contrasting hydrological-period patterns. Martinot et al. (2025) observed higher DOC concentrations during the wet period, whereas Nguyen et al. (2021) reported no significant differences between periods. In the present study, the lower DOC concentrations observed during the wet period may reflect dilution associated with high-discharge conditions. In contrast, higher DOC concentrations during the dry period may be favored by longer water residence times and enhanced in-river DOC accumulation.

As revealed by the PCA (Fig. 3), clear differences between the dry and wet hydrological periods were observed for CDOM parameters (Fig. 5). The total amount of CDOM was significantly higher during the wet period, with mean a(254) and a(350) values of 12.0±4.0 $m^{-1}$ and 4.8±2.2 $m^{-1}$, respectively, compared to the dry period. (6.7± 2.3 $m^{-1}$ and 1.9±0.8 $m^{-1}$) (U-test, $p < 0.0001$) (Fig. 5a, b; Table S5). In addition to these quantitative changes, CDOM quality also differed seasonally. $SUVA_{254}$ and $S_R$ values were significantly higher during the wet period (10.0±2.6 L mg $C^{-1}$ $m^{-1}$ and 1.3± 0.2, respectively) than during the dry period (4.3±0.8 L mg $C^{-1}$ $m^{-1}$ and 1.1±0.1) (U-test, $p < 0.0005$) (Fig. 5d, f). On the contrary, $E_2/E_3$ and $S_{275\text{-}295}$ values were significantly lower during the wet period (3.2±0.7 and 0.0108± 0.0018 $nm^{-1}$, respectively) than during the dry period (4.7±0.6 and 0.0137±0.0016 $nm^{-1}$, respectively) (U-test, $p < 0.0001$) (Fig. 5c, e; Table S5). These hydrological-period patterns are consistent with their distribution on the first PCA axis (Fig. 3) and with the correlations reported in Table S4. Higher $SUVA_{254}$ and lower $E_2/E_3$ and $S_{275\text{-}295}$ values during the wet period indicate a greater contribution of aromatic, high molecular weight terrestrial DOM (Helms et al., 2008; Kellerman et al., 2018; Weishaar et al., 2003). Together with the increase in CDOM abundance, these results are in agreement with enhanced terrestrial inputs associated with monsoon-driven runoff. Similar patterns were reported by Martinot et al. (2025).

As for CDOM, wet *vs.* dry period patterns were also marked for FDOM parameters. (Fig. 3; Fig. 6). The total amount of FDOM was significantly higher during the wet period, with mean fluorescence intensities of C1, C2 and C3 of 118±25 QSU, 418±85 QSU and 74±10 QSU, respectively, compared to the dry period, i.e., 66±29 QSU, 119±63 QSU and 47±23 QSU (U-test, $p < 0.0001$) (Fig. 6a-c; Table S5). Higher intensities of humic-like components (C1 and C3) during the wet period suggest enhanced inputs of terrestrially derived organic matter associated with monsoon-driven runoff and soil leaching within the Red River watershed. Concurrently, the increase in protein-like fluorescence (C2) suggests the transport of freshly produced microbial material and enhanced biological activity in Red River waters. Similar wet *vs.* dry period patterns have been reported in several river systems, particularly in large monsoon-influenced rivers (Han et al., 2021; Niloy et al., 2022; Zhang et al., 2023; Zheng et al., 2026).

On the other hand, fluorescence-based indices displayed significantly higher values in the dry period than in the rainy period: 0.77±0.14 *vs.* 0.64±0.02 for FI, 0.085±0.030 *vs.* 0.061±0.005 for BIX, and 2.2±1.9 *vs.* 1.3± 0.4 for HIX (U-test, $p < 0.0001$–$0.040$) (Fig. 6d-f; Table S5). Higher FI and BIX values during the dry period suggest a relatively greater contribution of autochthonous and microbially derived DOM, while higher HIX values indicate more extensive DOM processing under low-flow conditions and longer water residence times (Cory and McKnight, 2005; Fellman et al., 2010; Huguet et al., 2009; Ohno, 2002).

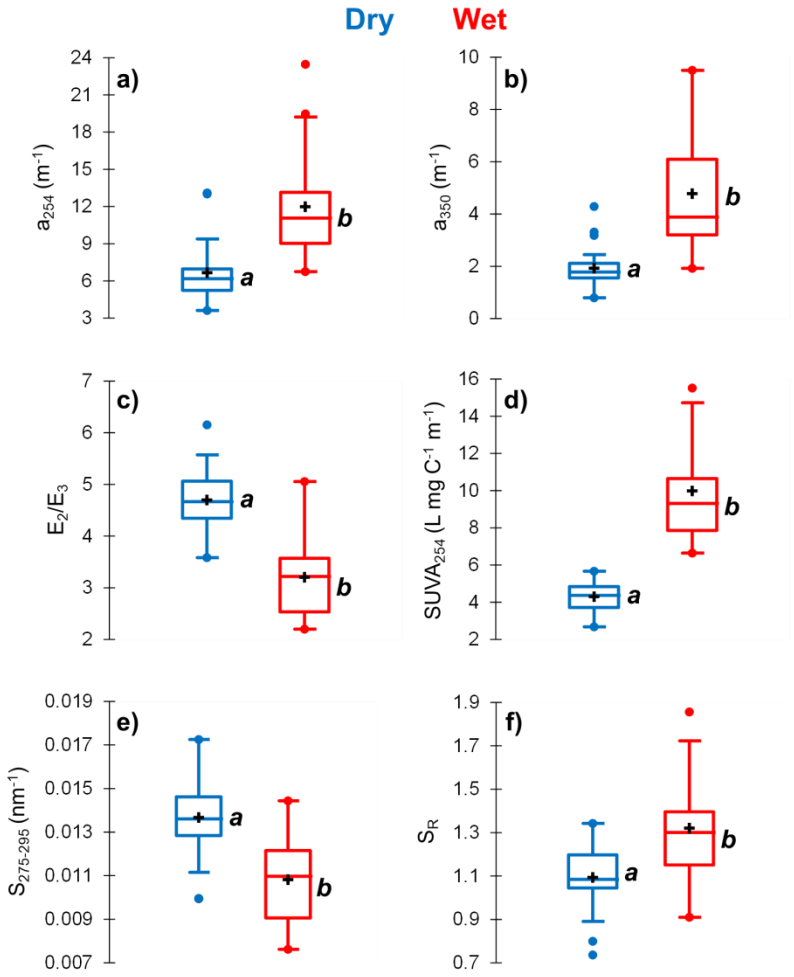


*Figure 5.* Distribution of CDOM parameters [a(254), a(350), $E_2/E_3$, $SUVA_{254}$, $S_{275-295}$, and $S_R$] according to hydrological period: dry (blue) and wet (red). Different letters indicate significant differences between periods (U-test, $p < 0.05$; Table S5)

Overall, DOM characteristics in the Red River showed marked differences between the dry and wet periods, highlighting the influence of monsoon-related hydrological conditions. While DOC concentrations were significantly higher during the dry period, CDOM and FDOM quantities were markedly higher during the wet period. This apparent discrepancy suggests a partial decoupling between DOM quantity and DOM optical properties. Indeed, optical measurements primarily characterize the chromophoric and fluorescent fractions of DOM, whereas DOC measurements integrate both optically active and non-chromophoric organic compounds (Massicotte et al., 2017; Spencer et al., 2012).

The elevated CDOM and FDOM levels observed during the wet period likely reflect enhanced inputs of terrestrially derived and microbially processed organic matter mobilized by monsoon runoff, soil leaching, and increased watershed connectivity. Such inputs are typically enriched in aromatic and humified compounds that contribute strongly to light absorption and fluorescence. In contrast, despite higher DOC concentrations during the

dry period, lower CDOM and FDOM intensities suggest a greater contribution of weakly chromophoric or non-chromophoric organic compounds to the bulk DOC pool.

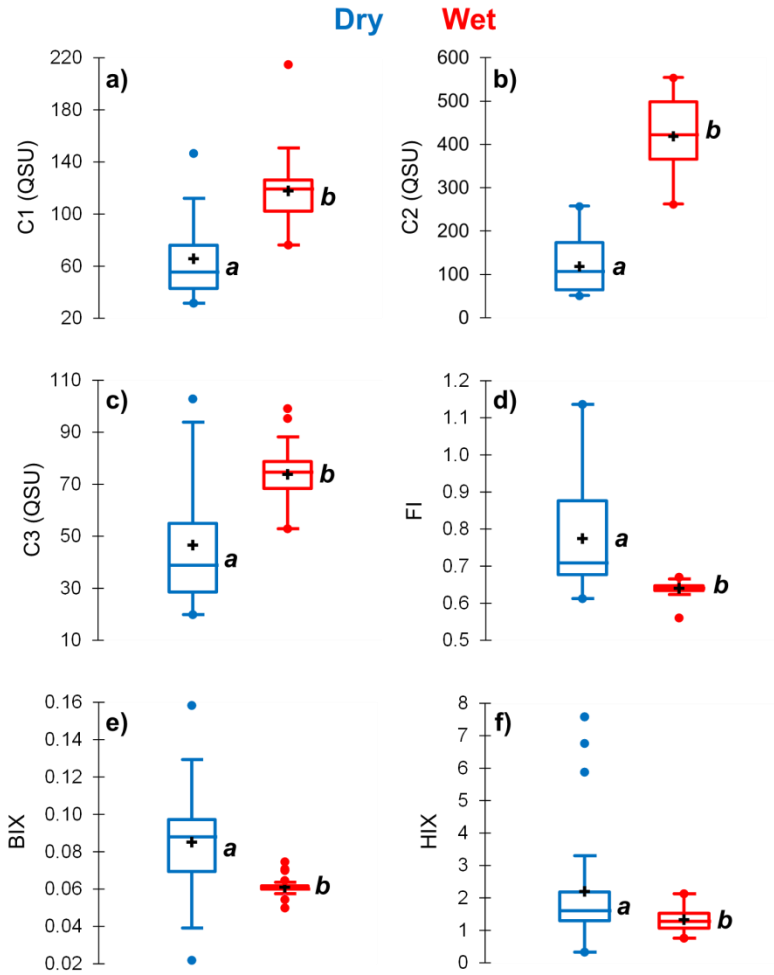


*Figure 6.* Distribution of FDOM parameters (C1, C2, C3, FI, BIX, and HIX) according to hydrological period: dry (blue) and wet (red). Different letters indicate significant differences between periods. (U-test, $p < 0.05$; Table S5)

Several mechanisms may contribute to this decoupling. First, longer water residence times during low-flow conditions may promote in-river biological production and microbial processing, generating relatively labile organic compounds that contribute to DOC but exhibit limited optical signatures (Lambert et al., 2016). Second, prolonged exposure of surface waters to solar radiation may enhance photobleaching and photodegradation of CDOM and FDOM, reducing their signals without necessarily causing proportional decreases in bulk DOC concentrations (Helms et al., 2008; Para et al., 2010). Finally, hydrological dilution and shifts in DOM source composition between the two sampling periods may further contribute to the observed divergence between DOC concentration and DOM optical properties (Hansen et al., 2016; Shin et al., 2016).

These observations indicate that changes in DOC concentration do not necessarily parallel

changes in DOM optical characteristics and highlight the importance of considering both DOM quantity and DOM quality when assessing carbon dynamics in monsoon-influenced river systems.

In addition to monsoon-related hydrological forcing, reservoir regulation may also influence DOM transport and transformation within the Red River basin. By increasing water residence times, reservoirs can promote sedimentation, microbial processing, and photochemical alteration of DOM before downstream export. Reservoir operations may also modify discharge variability and particulate transport during both low- and high-flow conditions. Although the influence of reservoir regulation was not specifically investigated in the present study, these processes could contribute to the observed differences between hydrological periods. They should be considered in future basin-scale investigations.

### *3.3. Spatial variability of CDOM and FDOM*

Spatial variations along the river continuum also play an important role in shaping DOM composition and sources. Rivers typically integrate multiple natural and anthropogenic inputs along their course, resulting in progressive transformations of DOM from upstream mountainous regions to downstream deltaic areas (Kamjunke et al., 2026; Lambert et al., 2016; Roebuck Jr. et al., 2020). In this basin, such spatial gradients are expected due to marked differences in land use, hydrological conditions, and human activities between the UpR and the densely populated RRD (Table 1). These gradients are expected to influence the distribution and transformation of DOM components along the river continuum.

Clear spatial differences were observed. DOC concentration, a(350) and a(254) (data not shown) were significantly higher in the UpR than in the RRD during both periods (U-test, p = 0.016–0.030) (Fig. 7a, b; Table S5). The intensities of C1 and C3 also tended to be higher in the UpR, although these differences were only significant during the wet period (U-test, p = 0.001–0.003) (Fig. 8a,c; Table S5). In contrast, C2 did not differ significantly between regions regardless of the period (U-test, p = 0.158–0.783) (Fig. 8b; Table S5), indicating relatively uniform sources of protein-like DOM. $S_{275\text{-}295}$ showed the opposite pattern, with higher values in the RRD, although not significantly during the wet period (Fig. 7c; Table S5), suggesting enhanced DOM degradation and lower molecular-weight compounds in downstream environments.

Higher DOC concentrations, CDOM absorption coefficients, and intensities of humic-like components in the UpR suggest a stronger influence of terrestrially derived organic matter originating from soils and vegetation in the forested mountainous watershed. Forested catchments indeed contain abundant leaf litter, decaying roots, plants, and soil organic matter that decompose gradually and produce humic and fulvic substances, resulting in DOM with higher aromaticity and molecular complexity (Fellman et al., 2010; Spencer et al., 2008; Wilson and Xenopoulos, 2009). This interpretation is further supported by the relatively high HIX values observed in the UpR during the dry period (Table S2), indicating a greater degree of humification. These results highlight the important role of forested headwaters as major sources of terrestrial DOM in the Red River system.

In contrast, the lower DOM concentrations observed in the RRD may result from dilution by tributaries and tidal waters, as well as enhanced in-river processing during downstream transport. Higher $S_{275\text{-}295}$ values in the RRD further support the presence of lower-molecular-weight, more photochemically or

microbially altered DOM, consistent with progressive degradation of terrestrially derived organic matter along the river continuum. It is worth noting that salinity gradients were absent in the UpR and became significant only near the Ba Lat estuary (see EC values in Table S1); therefore, variations in $S_{275\text{-}295}$ within the river are more likely related to changes in DOM composition rather than mixing processes. In addition, $SUVA_{254}$ showed a significant decrease from the UpR to the RRD, but only during the wet period (figure not shown). This downstream decrease, in line with the $S_{275\text{-}295}$ pattern, further indicates a reduction in DOM molecular weight and aromaticity along the Red River continuum, indicating substantial transformation of DOM during downstream transport (Helms et al., 2008; Martinot et al., 2025; Weishaar et al., 2003).

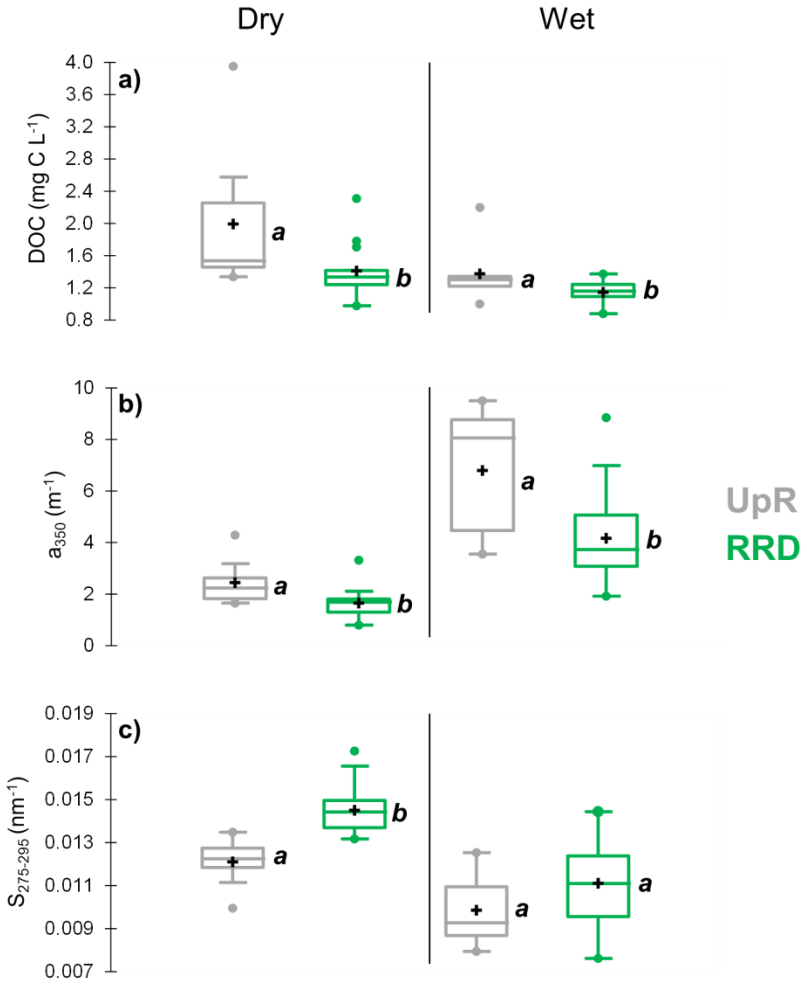


*Figure 7*. Distribution of DOC, a(350), and $S_{275\text{-}295}$ according to location: upstream region (UpR, grey) and Red River Delta (RRD, green). Different letters indicate significant differences between regions within each hydrological period (U-test, $p < 0.05$; Table S5)

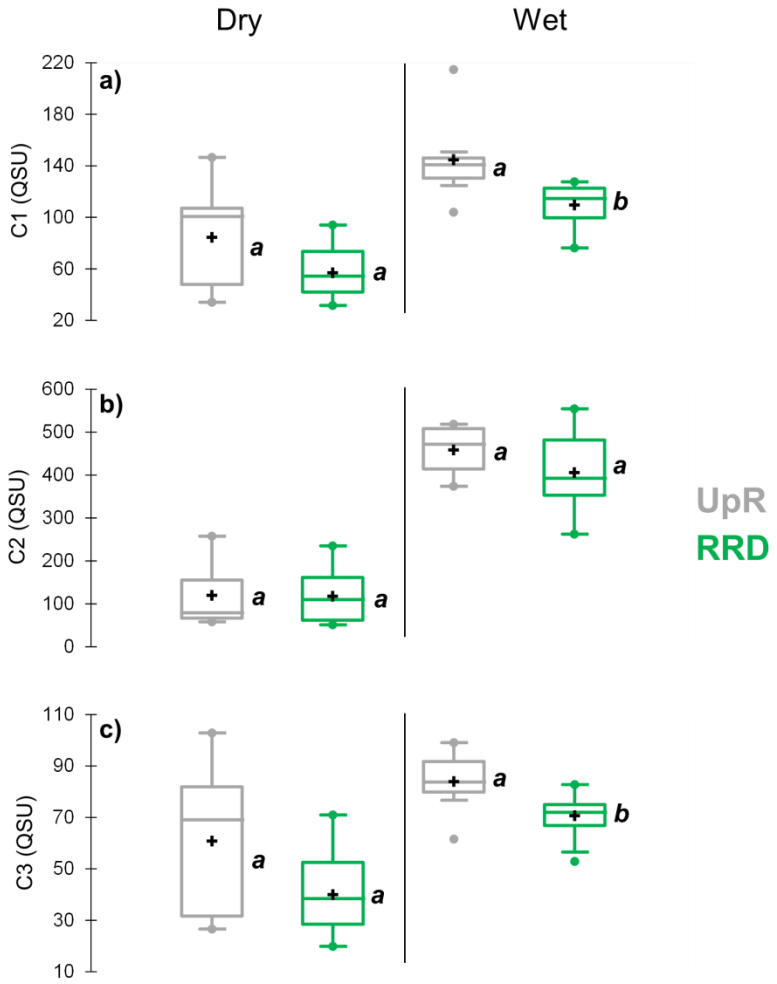


*Figure 8*. Distribution of FDOM components C1, C2, and C3 according to location: upstream region (UpR, grey) and Red River Delta (RRD, green). Different letters indicate significant differences between regions within each hydrological period (U-test, $p < 0.05$; Table S5)

The absence of significant spatial differences in the tryptophan-like component suggests that protein-like DOM is primarily controlled by *in situ* microbial activity rather than by watershed sources. Interestingly, the C2/C1 and C2/C3 ratios, as well as the relative contribution of C2 to total FDOM (%C2), were higher (although not significantly; Table S5) in the RRD than in the UpR, particularly during the dry period (Fig. 9a-c). This indicates that tryptophan-like DOM represented a greater proportion of the FDOM pool in downstream waters. This pattern suggests enhanced autochthonous production, driven by microbial activity and phytoplankton growth, under low-flow conditions, which can be favored by longer water residence times and increased nutrient availability in the deltaic region (Ferretto et al., 2017; Hosen et al., 2014; Lee and Kim, 2018).

In addition, the higher relative abundance of tryptophan-like fluorescence in the RRD might also be related in part to potential inputs of domestic wastewater effluents, which are known to contribute labile, protein-rich organic matter to river systems (Carstea et al., 2016; Hudson et al., 2007). Indeed, the RRD

includes densely populated areas where domestic wastewater discharges may potentially contribute to the higher proportion of protein-like DOM observed. This hypothesis is in accordance with previous studies showing that protein-like fluorescence is typically more abundant in urban or sewage-impacted rivers/coastal waters (Hudson et al., 2007; Parr et al., 2015; Tedetti et al., 2012). Agricultural practices, such as the application of organic fertilizers and pesticides, may also contribute to elevated protein-like DOM through runoff and soil erosion (Osburn et al., 2016; Vu et al., 2023). However, because no direct anthropogenic tracers (e.g., fecal indicators, wastewater markers, isotopic tracers or microbial abundance) were measured in the present study, potential contributions from wastewater discharges or agricultural runoff cannot be distinguished from natural biological production. Consequently, these interpretations should be regarded as plausible hypotheses rather than demonstrated mechanisms.

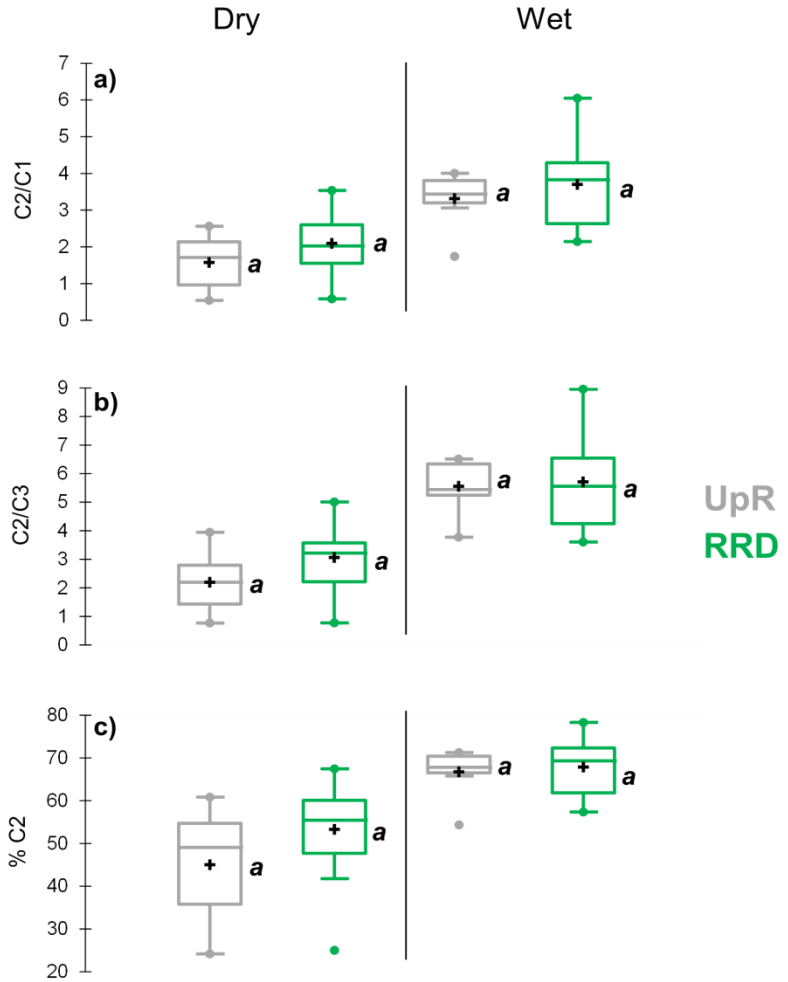


*Figure 9*. Distribution of the C2/C1 ratio, C2/C3 ratio, and the relative contribution of C2 to total FDOM (%C2) according to location: upstream region (UpR, grey) and Red River Delta (RRD, green). No significant differences were observed between regions within either hydrological period (U-test, $p > 0.05$; Table S5)

Although the UpR-RRD classification proved useful for investigating large-scale longitudinal gradients in DOM characteristics, it necessarily simplifies the spatial complexity of the Red River system. In particular, the deltaic region encompasses a mosaic of urbanized areas, agricultural landscapes, distributary channels, and estuarine environments that may exhibit distinct sources and transformations of DOM. Consequently, local-scale variability within the RRD may not be fully resolved by the present regional-scale approach. Furthermore, although salinity was not measured directly, elevated EC values observed at the most downstream station (St 34; Table S1) indicate saline intrusion during the dry period, suggesting that estuarine mixing may influence DOM concentrations and optical properties near the Ba Lat estuary. Because this station was retained as the downstream end-member of the river continuum, its DOM characteristics likely reflect both riverine and estuarine influences. Future studies with higher spatial resolution and dedicated salinity-based mixing analyses could further investigate DOM dynamics across specific land-use types and hydrological settings within the delta and estuarine zone.

## 4. Conclusions

This study provides a comprehensive characterization of CDOM and FDOM dynamics in the Red River by combining optical and fluorescence analyses across contrasting hydrological conditions and along the river continuum. PARAFAC modeling revealed a FDOM pool composed of two humic-like components (C1 and C3), mainly associated with terrestrially derived organic matter, and one tryptophan-like component (C2), indicative of recently produced and labile material of microbial origin.

Our results reveal marked differences in DOM optical properties between the dry- and wet-period sampling campaigns, suggesting a significant influence of hydrological conditions associated with the monsoon regime. During the wet period, increased river discharge enhances the export of terrestrially derived organic matter from the watershed, resulting in higher concentrations of CDOM and FDOM, greater aromaticity, and higher molecular-weight DOM. In contrast, the dry period is characterized by lower DOM concentrations but relatively higher contributions of autochthonous and microbially processed material, reflecting longer water residence times, enhanced *in situ* production, and increased photochemical and microbial alteration.

In addition to the differences observed between contrasting hydrological periods, marked spatial gradients were observed along the upstream-downstream continuum. The UpR is dominated by terrestrially derived, humified DOM originating from forested catchments, whereas the RRD exhibits lower DOM concentrations and more processed material, consistent with dilution, degradation, and transformation during downstream transport. The relatively higher contribution of tryptophan-like DOM in the delta may reflect enhanced autochthonous production and/or possible anthropogenic contributions associated with downstream land use. However, additional tracers would be required to distinguish between these potential sources.

Finally, this work highlights the combined roles of contrasting hydrological conditions, in-river processing, and potential anthropogenic influences in shaping CDOM and FDOM characteristics in a large monsoon-influenced river system. These findings improve our understanding of DOM dynamics and carbon cycling in Southeast Asian rivers and underscore the importance of accounting for both hydrological-period and spatial variability when assessing DOM sources, transformations, and export to coastal

waters. However, because this study is based on two discrete field campaigns, the observed patterns should be interpreted as representative snapshots of contrasting hydrological conditions rather than exhaustive seasonal dynamics.

Future studies combining optical analyses with molecular, microbial, and isotopic tracers, as well as higher temporal-resolution monitoring, would further improve our understanding of DOM sources, transformation processes, hydrological controls, including reservoir regulation, and land-river-ocean carbon transfer in the Red River system under increasing anthropogenic and climatic pressures.

## Acknowledgments

This study was funded by the Vietnam Academy of Science and Technology (VAST; project code: QTFR02.03/24-25) for data interpretation, analysis, and manuscript preparation, as well as for PhD support Thi Quynh Mai Duong (No. 77/QĐ-ĐHKHCN, date 14 January 2025) on behalf of Cotutelle doctoral program between University of Science and Technology of Hanoi (USTH), Vietnam and Aix Marseille University (AMU), France. This work also contributes to the IRD International Joint Laboratory "LOTUS" (2019-2027) and the IRD International Research Network "SOOT-SEA" (2018-2026), both supported by the French National Research Institute for Sustainable Development (IRD), France. These programs provided support for study design, field sample collection, and laboratory analyses. The authors gratefully acknowledge all colleagues and technicians, as well as the students involved in the fieldwork and laboratory analyses. We warmly thank two anonymous reviewers and the Editor-in-Chief for their relevant and helpful comments and corrections.

## References

Andrew A.A., Del Vecchio R., Subramaniam A., Blough N.V., 2013. Chromophoric dissolved organic matter (CDOM) in the Equatorial Atlantic Ocean: Optical properties and their relation to CDOM structure and source. Marine Chemistry, 148, 33–43. https://doi.org/10.1016/j.marchem.2012.11.001.

Bricaud A., Morel A., Prieur L., 1981. Absorption by dissolved organic matter of the sea (yellow substance) in the UV and visible domains. Limnology and Oceanography, 26(1), 43–53. https://doi.org/10.4319/lo.1981.26.1.0043.

Carstea E.M., Bridgeman J., Baker A., Reynolds D.M., 2016. Fluorescence spectroscopy for wastewater monitoring: A review. Water Research, 95, 205–219. https://doi.org/10.1016/j.watres.2016.03.021.

Coble, P.G., 1996. Characterization of marine and terrestrial DOM in seawater using excitation-emission matrix spectroscopy. Marine Chemistry, 51(4), 325–346. https://doi.org/10.1016/0304-4203(95)00062-3.

Coble P.G., 2007. Marine Optical Biogeochemistry: The Chemistry of Ocean Color. Chemical Reviews 107(2), 402–418. https://doi.org/10.1021/cr050350+.

Coble P.G., Lead J., Baker A. (Eds.), 2014. Aquatic organic matter fluorescence. Cambridge University Press. Aquatic organic matter fluorescence. Cambridge Environmental Chemistry Series, Cambridge University Press, New York, NY, USA, 75–122.

Cory R.M., McKnight D.M., 2005. Fluorescence spectroscopy reveals ubiquitous presence of oxidized and reduced quinones in dissolved organic matter. Environmental Science and Technology, 39(21), 8142–8149. https://doi.org/10.1021/es0506962.

D'Andrilli J., Silverman V., Buckley S., Rosario-Ortiz F.L., 2022. Inferring ecosystem function from dissolved organic matter optical properties: a critical review. Environmental Science and Technology, 56(16), 11146–11161. https://doi.org/10.1021/acs.est.2c04240.

De Haan H., De Boer T., 1987. Applicability of light absorbance and fluorescence as measures of concentration and molecular size of dissolved

organic carbon in humic Lake Tjeukemeer. Water research, 21(6), 731–734. https://doi.org/10.1016/0043-1354(87)90086-8.

Dittmar T., Lennartz S.T., Buck-Wiese H., Hansell D.A., Santinelli C., Vanni C., Blasius B., Hehemann J.-H., 2021. Enigmatic persistence of dissolved organic matter in the ocean. Nature Reviews Earth and Environment, 2, 570–583. https://doi.org/10.1038/s43017-021-00183-7.

Dittmar T., Stubbins A., 2014. Dissolved organic matter in aquatic systems, In: H.D. Holland, K.K. Turekian (Eds.), Treatise on Geochemistry, Second edition. Elsevier Science, 2, 125–156. http://dx.doi.org/10.1016/B978-0-08-095975-7.01010-X.

Duursma E.K., 1974. The fluorescence of dissolved organic matter in the sea, In: N.G. Jerlov, E. Steemann Nielsen (Eds.), Optical Aspects of Oceanography. Academic Press, New York, 237–256.

Fabre C., Wei X., Sauvage S., Le T.P.Q., Ouillon S., Orange D., Herrmann M., Sánchez-Pérez J.-M., 2023. Assessing fluvial organic carbon flux and its response to short climate variability and damming on a large-scale tropical Asian river basin. Science of The Total Environment, 903, 166589. https://doi.org/10.1016/j.scitotenv.2023.166589.

Fellman J.B., Hood E., Spencer R.G.M., 2010. Fluorescence spectroscopy opens new windows into dissolved organic matter dynamics in freshwater ecosystems: A review. Limnology and Oceanography, 55(6), 2452–2462. https://doi.org/10.4319/lo.2010.55.6.2452.

Ferretto N., Tedetti M., Guigue C., Mounier S., Raimbault, P., Goutx, M., 2017. Spatio-temporal variability of fluorescent dissolved organic matter in the Rhône River delta and the Fos-Marseille marine area (France, NW Mediterranean Sea). Environmental Science and Pollution Research, 24(5), 4973–4989. https://doi.org/10.1007/s11356-016-8255-z.

Fourrier P., Dulaquais G., Guigue C., Giamarchi P., Sarthou G., Whitby H., Riso R., 2022. Characterization of the vertical size distribution, composition and chemical properties of dissolved organic matter in the (ultra)oligotrophic Pacific Ocean through a multi-detection approach. Marine Chemistry, 240, 104068. https://doi.org/10.1016/j.marchem.2021.104068.

Han Z., Xiao M., Yue F., Yi Y., Mostofa K.M.G., 2021. Seasonal Variations of Dissolved Organic Matter by Fluorescent Analysis in a Typical River Catchment in Northern China. Water, 13, 494. https://doi.org/10.3390/w13040494.

Hansen A.M., Kraus T.E.C., Pellerin B.A., Fleck J.A., Downing B.D., Bergamaschi B.A., 2016. Optical properties of dissolved organic matter (DOM): Effects of biological and photolytic degradation. Limnology and Oceanography, 61(3), 1015–1032. https://doi.org/10.1002/lno.10270.

Helms J.R., Stubbins A., Ritchie J.D., Minor E.C., Kieber D.J., Mopper K., 2008. Absorption spectral slopes and slope ratios as indicators of molecular weight, source and photobleaching of chromophoric dissolved organic matter. Limnology and Oceanography, 53(3), 955–969. https://doi.org/10.4319/lo.2008.53.3.0955.

Hosen J.D., Aho K.S., Fair J.H., Kyzivat E.D., Matt S., Morrison J., Stubbins A., Weber L.C., Yoon B., Raymond P.A., 2021. Source Switching Maintains Dissolved Organic Matter Chemostasis Across Discharge Levels in a Large Temperate River Network. Ecosystems, 24(2), 227–247. https://doi.org/10.1007/s10021-020-00514-7.

Hosen J.D., McDonough O.T., Febria C.M., Palmer M.A., 2014. Dissolved organic matter quality and bioavailability changes across an urbanization gradient in headwater streams. Environmental Science and Technology, 48(14), 7817–7824. https://doi.org/10.1021/es501422z.

Hudson N., Baker A., Reynolds D., 2007. Fluorescence analysis of dissolved organic matter in natural, waste and polluted waters a review. River Res. Applic., 23(6), 631–649. https://doi.org/10.1002/rra.1005.

Huguet A., Vacher L., Relexans S., Saubusse S., Froidefond J.M., Parlanti E., 2009. Properties of fluorescent dissolved organic matter in the Gironde Estuary. Organic Geochemistry, 40(6), 706–719. https://doi.org/10.1016/j.orggeochem.2009.03.002.

Huong P.T.T., Everaarts A.P., Neeteson J.J., Struik P.C., 2013. Vegetable production in the Red River Delta

of Vietnam. II. Profitability, labour requirement and pesticide use. NJAS - Wageningen Journal of Life Sciences 67, 37–46. https://doi.org/10.1016/j.njas.2013.09.003.

Ishii S.K.L., Boyer T.H., 2012. Behavior of Reoccurring PARAFAC Components in Fluorescent Dissolved Organic Matter in Natural and Engineered Systems: A Critical Review. Environmental Science and Technology, 46(6), 2006–2017. https://doi.org/10.1021/es2043504.

Jaffé R., Ding Y., Niggemann J., Vähätalo A.V., Stubbins A., Spencer R.G., Campbell J., Dittmar T., 2013. Global charcoal mobilization from soils via dissolution and riverine transport to the oceans. Science, 340(6130), 345–347. https://doi.org/10.1126/science.1231476.

Jaffé R., Cawley K.M., Yamashita Y., 2014. Applications of excitation emission matrix fluorescence with parallel factor Analysis (EEM-PARAFAC) in assessing environmental dynamics of natural dissolved organic matter (DOM) in aquatic environments: a review, In: Advances in the Physicochemical Characterization of Dissolved Organic Matter: Impact on Natural and Engineered Systems. American Chemical Society, 27–73. https://doi.org/10.1021/bk-2014-1160.ch003.

Kang W., Hu X., Feng R., Wei C., Yu F., 2023. DOM associates with greenhouse gas emissions in Chinese rivers under diverse land uses. Environmental Science and Technology, 57(40), 15004–15013. https://doi.org/10.1021/acs.est.3c03826.

Kellerman A.M., Guillemette F., Podgorski D.C., Aiken G.R., Butler K.D., Spencer R.G.M., 2018. Unifying Concepts Linking Dissolved Organic Matter Composition to Persistence in Aquatic Ecosystems. Environmental Science and Technology, 52(5), 2538–2548. https://doi.org/10.1021/acs.est.7b05513.

Korak J.A., McKay G., 2024. Critical review of fluorescence and absorbance measurements as surrogates for the molecular weight and aromaticity of dissolved organic matter. Environmental Science: Processes & Impacts, 26(10), 1663–1702. https://doi.org/10.1039/d4em00183d.

Kamjunke N., Herzsprung P., von Tümpling W., Matoušů A., Znachor P., Sanders T., Brix H., Bussmann I., Weitere M., Lechtenfeld O.J., 2026. Longitudinal dynamics and transformation of riverine dissolved organic matter from source to sea. Water Research, 288, 124613. https://doi.org/10.1016/j.watres.2025.124613.

Laane R.W.P.M., Koole L., 1982. The relation between fluorescence and dissolved organic carbon in the Ems-Dollart estuary and the Western Wadden Sea. Netherlands Journal of Sea Research, 15(2), 217–227. https://doi.org/10.1016/0077-7579(82)90005-9.

Lambert T., Teodoru C.R., Nyoni F.C., Bouillon S., Darchambeau F., Massicotte P., Borges A.V., 2016. Along-stream transport and transformation of dissolved organic matter in a large tropical river. Biogeosciences, 13(9), 2727–2741. https://doi.org/10.5194/bg-13-2727-2016.

Le N.D., Le T.P.Q., Phung T.X.B., Duong T.T., Didier O., 2020. Impact of hydropower dam on total suspended sediment and total organic nitrogen fluxes of the Red River (Vietnam). Proceedings of the International Association of Hydrological Sciences, 383, 367–374. https://doi.org/10.5194/piahs-383-367-2020.

Le T.P.Q., Billen G., Garnier J., Chau V.M., 2015. Long-term biogeochemical functioning of the Red River (Vietnam): past and present situations. Regional Environmental Change, 15(2), 329–339. https://doi.org/10.1007/s10113-014-0646-4.

Le T.P.Q., Dao V.N., Rochelle-Newall E., Garnier J., Lu X., Billen G., Duong T.T., Ho C.T., Etcheber H., Nguyen T.M.H., Nguyen T.B.N., Nguyen B.T., Da Le N., Pham Q.L., 2017. Total organic carbon fluxes of the Red River system (Vietnam): TOC fluxes of the Red River. Earth Surface Processes and Landforms 42(9), 1329–1341. https://doi.org/10.1002/esp.4107.

Le T.P.Q., Garnier J., Gilles B., Sylvain T., Van Minh C., 2007. The changing flow regime and sediment load of the Red River, Viet Nam. Journal of Hydrology, 334(1–2), 199–214. https://doi.org/10.1016/j.jhydrol.2006.10.020.

Shin-Ah L., Kim G., 2018. Sources, fluxes, and behaviors of fluorescent dissolved organic matter (FDOM) in the Nakdong River Estuary, Korea. Biogeosciences, 15(4), 1115–1122. https://doi.org/10.5194/bg-15-1115-2018.

Lee M.-H., Osburn C.L., Shin K.-H., Hur J., 2018. New insight into the applicability of spectroscopic indices for dissolved organic matter (DOM) source discrimination in aquatic systems affected by biogeochemical processes. Water Research, 147, 164–176. https://doi.org/10.1016/j.watres.2018.09.048.

Leenheer J.A., Croué J.P., 2003. Characterizing aquatic dissolved organic matter. Environmental Science and Technology, 37(1), 18A–26A. https://doi.org/10.1021/es032333c.

Li P., Hur J., 2017. Utilization of UV-Vis spectroscopy and related data analyses for dissolved organic matter (DOM) studies: A review. Critical Reviews in Environmental Science and Technology, 47(3), 131–154. https://doi.org/10.1080/10643389.2017.1309186.

Lin H., Guo L., 2020. Variations in colloidal DOM composition with molecular weight within individual water samples as characterized by flow field-flow fractionation and EEM-PARAFAC analysis. Environmental Science & Technology, 54(3), 1657–1667. https://doi.org/10.1021/acs.est.9b07123.

Luu T.N.M., Garnier J., Billen G., Le T.P.Q., Némery J., Orange D., Le L.A., 2012. N, P, Si budgets for the Red River Delta (Northern Vietnam): How the delta affects river nutrient deliveries to the sea. Biogeochemistry, 107(1), 241–259. https://doi.org/10.1007/s10533-010-9549-8.

Martinot P.L, Guigue C., Bui V.H., Gourdon L., Mari X., Canh N.T., Dang V.Q.D., Duong T.Q.M., Tedetti M., Vu C.T., 2025. Seasonal and spatial variability of dissolved black carbon in the Red River delta (North Vietnam). Biogeochemistry 168(6), 85. https://doi.org/10.1007/s10533-025-01278-9.

Massicotte P., Asmala E., Stedmon C., Markager S., 2017. Global distribution of dissolved organic matter along the aquatic continuum: Across rivers, lakes and oceans. Science of The Total Environment, 609, 180–191. https://doi.org/10.1016/j.scitotenv.2017.07.076.

McKnight D.M., Boyer E.W., Westerhoff P.K., Doran P.T., Kulbe T., Andersen D.T., 2001. Spectrofluorometric characterization of dissolved organic matter for indication of precursor organic material and aromaticity. Limnology and Oceanography, 46(1), 38–48. https://doi.org/10.4319/lo.2001.46.1.0038.

Mielnik L., Kowalczuk P., 2018. Optical characteristic of humic acids from lake sediments by excitation-emission matrix fluorescence with PARAFAC model. Journal of Soils and Sediments, 18(8), 2851–2862. https://doi.org/10.1007/s11368-018-1947-x.

Murphy K.R., Stedmon C.A., Waite T.D., Ruiz G.M., 2008. Distinguishing between terrestrial and autochthonous organic matter sources in marine environments using fluorescence spectroscopy. Marine Chemistry, 108(1–2), 40–58. https://doi.org/10.1016/j.marchem.2007.10.003.

Murphy K.R., Stedmon C.A., Wenig P., Bro R., 2014. OpenFluor an online spectral library of auto-fluorescence by organic compounds in the environment. Analytical methods, 6(3), 658–661. https://doi.org/10.1039/c3ay41935e.

Nelson N.B., Siegel D.A., 2013. The global distribution and dynamics of chromophoric dissolved organic matter. Annual review of marine science, 5(1), 447–476. https://doi.org/10.1146/annurev-marine-120710-100751.

Nelson N.B., Siegel D.A., Carlson C.A., Swan C., Smethie Jr W.M., Khatiwala S., 2007. Hydrography of chromophoric dissolved organic matter in the North Atlantic. Deep Sea Research Part I: Oceanographic Research Papers, 54(5), 710–731. https://doi.org/10.1016/j.dsr.2007.02.006.

Niloy N.M., Shammi M., Haque M.M., Tareq S.M., 2022. Investigating dissolved organic matter dynamics in the downstream reaches of the Ganges

and Brahmaputra Rivers using fluorescence spectroscopy. Frontiers in Earth Science, 10, 821050. https://doi.org/10.3389/feart.2022.821050.

Nguyen H.D., Dang D.K., Lai T.A.T., Tran D.D., Shahabi H., Bui Q.T., 2025. Predicting Soil Salinity in the Red River Delta (Vietnam) Using Machine Learning and Assessing Farmers' Adaptive Capacity. Natural Hazards and Earth System Sciences, 25(9), 3505–3524. https://doi.org/10.5194/nhess-25-3505-2025.

Nguyen H.Q., Tran Q.V., 2023. Long-term analysis of sediment load changes in the Red River system (Vietnam) due to dam-reservoirs. Journal of Hydro-environment Research, 51, 48–66. https://doi.org/10.1016/j.jher.2023.10.002.

Nguyen T.M.H., Le T.P.Q., Hoang V.V., Vu C.T., 2022. Biodegradable and Seasonal Variation of Organic Carbon Affected by Anthropogenic Activity: A Case in Xuan Thuy Mangrove Forest, North Vietnam. Water, 14(5), 773. https://doi.org/10.3390/w14050773.

Nguyen T.M.H., Le T.P.Q., Van Hoang V., Nhu D.L., Vu C.T., Thi Thuy D., 2021. Seasonal and spatial variation in biodegradability of organic carbon along the Red River, Vietnam. Carbon Management, 12(5), 549–557. https://doi.org/10.1080/17583004.2021.1980110.

Obrador B., von Schiller D., Marcé R., Gómez-Gener L., Koschorreck M., Borrego C., Catalán N., 2018. Dry habitats sustain high $CO_2$ emissions from temporary ponds across seasons. Scientific Reports, 8(1), 3015. https://doi.org/10.1038/s41598-018-20969-y.

Ohno T., 2002. Fluorescence inner-filtering correction for determining the humification index of dissolved organic matter. Environmental Science and Technology, 36(4), 742–746. https://doi.org/10.1021/es0155276.

Osburn C.L., Handsel L.T., Peierls B.L., Paerl H.W., 2016. Predicting sources of dissolved organic nitrogen to an estuary from an agro-urban coastal watershed. Environmental Science and Technology, 50(16), 8473–8484. https://doi.org/10.1021/acs.est.6b00053.

Para J., Coble P.G., Charrière B., Tedetti M., Fontana C., Sempere R., 2010. Fluorescence and absorption properties of chromophoric dissolved organic matter (CDOM) in coastal surface waters of the northwestern Mediterranean Sea, influence of the Rhône River. Biogeosciences, 7(12), 4083–4103. https://doi.org/10.5194/bg-7-4083-2010.

Parr T.B., Cronan C.S., Ohno T., Findlay S.E.G., Smith S.M.C., Simon K.S., 2015. Urbanization changes the composition and bioavailability of dissolved organic matter in headwater streams. Limnology and Oceanography, 60(3), 885–900. https://doi.org/10.1002/lno.10060.

Park J.H., Jin H., Yoon T.K., Begum M.S., Eliyan C., Lee E.-J., Lee S.-C., Oh N.-H., 2021. Wastewater-boosted biodegradation amplifying seasonal variations of $pCO_2$ in the Mekong-Tonle Sap river system. Biogeochemistry, 155(2), 219–235. https://doi.org/10.1007/s10533-021-00823-6.

Parlanti E., Worz K., Geoffroy L., Lamotte M., 2000. Dissolved organic matter fluorescence spectroscopy as a tool to estimate biological activity in a coastal zone submitted to anthropogenic inputs. Organic Geochemistry, 31(12), 1765–1781. https://doi.org/10.1016/S0146-6380(00)00124-8.

Peuravuori J., Pihlaja K., 1997. Molecular size distribution and spectroscopic properties of aquatic humic substances. Analytica Chimica Acta, 337(2), 133–149. https://doi.org/10.1016/S0003-2670(96)00412-6.

Piton V., Ouillon S., Vinh V.D., Many G., Herrmann M., Marsaleix P., 2020. Seasonal and tidal variability of the hydrology and suspended particulate matter in the Van Uc estuary, Red River, Vietnam. Journal of Marine Systems, 211, 103403. https://doi.org/10.1016/j.jmarsys.2020.103403.

Redfern S.K., Azzu N., Binamira J.S., 2012. Rice in Southeast Asia: facing risks and vulnerabilities to respond to climate change. Build Resilience Adapt Climate Change Agri Sector. Proceedings of a Joint FAO/OECD Workshop 23–24 April 2012, 23(295), 1–14. http://www.fao.org/docrep/017/i3084e/i3084e18.pdf

Brogi S.R., Balestra C., Casotti R., Cossarini G., Galletti Y., Gonnelli M., Vestri S., Santinelli C., 2020. Time resolved data unveils the complex DOM dynamics in a Mediterranean river. Science of the Total Environment, 733, 139212. https://doi.org/10.1016/j.scitotenv.2020.139212.

Roebuck Jr J.A., Seidel M., Dittmar T., Jaffé R., 2020. Controls of Land Use and the River Continuum Concept on Dissolved Organic Matter Composition in an Anthropogenically Disturbed Subtropical Watershed. Environmental Science and Technology, 54(1), 195–206. https://doi.org/10.1021/acs.est.9b04605.

Shi Y., Zhang L., Li Y., Zhou L., Zhou Y., Zhang Y., Huang C., Li H., Zhu G., 2020. Influence of land use and rainfall on the optical properties of dissolved organic matter in a key drinking water reservoir in China. Science of the Total Environment, 699, 134301. https://doi.org/10.1016/j.scitotenv.2019.13430.

Shin Y., Lee E.-J., Jeon Y.-J., Hur J., Oh N.-H., 2016. Hydrological changes of DOM composition and biodegradability of rivers in temperate monsoon climates. Journal of Hydrology, 540, 538–548. https://doi.org/10.1016/j.jhydrol.2016.06.004.

Sohrin R., Sempéré R., 2005. Seasonal variation in total organic carbon in the northeast Atlantic in 2000–2001. Journal of Geophysical Research: Oceans, 110(C10). https://doi.org/10.1029/2004JC002731.

Spencer R.G., Aiken G.R., Wickland K.P., Striegl R. G., Hernes P.J., 2008. Seasonal and spatial variability in dissolved organic matter quantity and composition from the Yukon River basin, Alaska. Global Biogeochemical Cycles, 22(4). https://doi.org/10.1029/2008GB003231.

Spencer R.G., Butler K.D., Aiken G.R., 2012. Dissolved organic carbon and chromophoric dissolved organic matter properties of rivers in the USA. Journal of Geophysical Research: Biogeosciences, 117(G3). https://doi.org/10.1029/2011JG001928.

Stedmon C.A., Bro R., 2008. Characterizing dissolved organic matter fluorescence with parallel factor analysis: a tutorial. Limnology and Oceanography: Methods, 6(11), 572–579. https://doi.org/10.4319/lom.2008.6.572.

Stedmon C.A., Cory R.M., 2014. Biological origins and fate of fluorescent dissolved organic matter in aquatic environments, In: P.G. Coble, J. Lead, A. Baker, D.M. Reynolds, R.G.M. Spencer (Eds.), Aquatic organic matter fluorescence. Cambridge Environmental Chemistry Series, Cambridge University Press, New York, NY, USA, 278–299.

Stedmon C.A., Markager S., 2005. Resolving the variability of dissolved organic matter fluorescence in a temperate estuary and its catchment using PARAFAC analysis. Limnology and Oceanography, 50(2), 686–697. https://doi.org/10.4319/lo.2005.50.2.0686.

Stedmon C.A., Markager S., Bro R., 2003. Tracing dissolved organic matter in aquatic environments using a new approach to fluorescence spectroscopy. Marine Chemistry, 82(3–4), 239–254. https://doi.org/10.1016/S0304-4203(03)00072-0.

Tedetti M., Guigue C., Mahieu L., Martinot P.L., Benavides M., Dupouy C., Nunige S., Pulido-Villena E., Dimier C., Tilliette C., Bonnet S., Guieu C., Lefèvre D., 2026. Dissolved organic matter (DOC, CDOM, FDOM) in the Western Tropical South Pacific: Depth- and subregion-resolved variability, and hydrothermal influence. Progress in Oceanography, 242, 103664. https://doi.org/10.1016/j.pocean.2025.103664.

Tedetti M., Longhitano R., Garcia N., Guigue C., Ferretto N., Goutx M., 2012. Fluorescence properties of dissolved organic matter in coastal Mediterranean waters influenced by a municipal sewage effluent (Bay of Marseilles, France). Environmental Chemistry, 9(5), 438–449. https://doi.org/10.1071/EN12081.

Twardowski M.S., Boss E., Sullivan J.M., Donaghay P.L., 2004. Modeling the spectral shape of absorption by chromophoric dissolved organic matter. Marine Chemistry, 89(1–4), 69–88. https://doi.org/10.1016/j.marchem.2004.02.008.

Vinh V.D., Ouillon S., Thanh T.D., Chu L., 2014. Impact of the Hoa Binh dam (Vietnam) on water and sediment budgets in the Red River basin and delta. Hydrology and Earth System Sciences, 18(10), 3987–4005. https://doi.org/10.5194/hess-18-3987-2014.

Vu C.T., Chu D.B., Mai H., Herrmann M., Bui V.H., Le P.T., Chu N.H.A., Tedetti M., Behra P., 2023. First hydrological study on the seasonal occurrence of glyphosate, glufosinate, and their metabolites in the Red River system, North Vietnam. Environmental Nanotechnology, Monitoring and Management, 20, 100833. https://doi.org/10.1016/j.enmm.2023.100833.

Wei X., Sauvage S., Le T.P.Q., Ouillon S., Orange D., Vinh V.D., Sanchez-Perez J.-M., 2019. A Modeling Approach to Diagnose the Impacts of Global Changes on Discharge and Suspended Sediment Concentration within the Red River Basin. Water, 11(5), 958. https://doi.org/10.3390/w11050958.

Weishaar J.L., Aiken G.R., Bergamaschi B.A., Fram M.S., Fujii R., Mopper K., 2003. Evaluation of specific ultraviolet absorbance as an indicator of the chemical composition and reactivity of dissolved organic carbon. Environmental Science and Technology, 37(20), 4702–4708. https://doi.org/10.1021/es030360x.

Wilson H., Xenopoulos M., 2009. Effects of agricultural land use on the composition of fluvial dissolved organic matter. Nature Geoscience, 2(1), 37–41. https://doi.org/10.1038/ngeo391.

Xue L.I., Yungang L.I., Jiaonan H.E., Xian L.U.O., 2016. Analysis of variation in runoff and impacts factors in the Yuanjiang-Red River Basin from 1956 to 2013. Resources Science, 38(6), 1149–1159. https://doi.org/10.18402/resci.2016.06.14.

Yamashita Y., Maie N., Briceño H., Jaffé R., 2010. Optical characterization of dissolved organic matter in tropical rivers of the Guayana Shield, Venezuela. Journal of Geophysical Research: Biogeosciences, 115(G1). https://doi.org/10.1029/2009JG000987.

Yamashita Y., Nosaka Y., Suzuki K., Ogawa H., Takahashi K., Saito H., 2013. Photobleaching as a factor controlling spectral characteristics of chromophoric dissolved organic matter in open ocean. Biogeosciences, 10(11), 7207–7217. https://doi.org/10.5194/bg-10-7207-2013.

Yan P., Wei S., Chen Y., Ning Q., Hu Z., Guo Z., Xie H., Wu H., Zhang J., 2023. Fluorescence spectroscopic characterization of dissolved organic matter in the wastewater treatment plant and hybrid constructed wetlands coupling system in winter: A case study in eastern China. Environmental Technology and Innovation, 32, 103399. https://doi.org/10.1016/j.eti.2023.103399.

Yuen K.W., Hanh T.T., Quynh V.D., Switzer A.D., Teng P., Lee J.S.H., 2021. Interacting effects of land-use change and natural hazards on rice agriculture in the Mekong and Red River deltas in Vietnam. Natural Hazards and Earth System Sciences, 21(5), 1473–1493. https://doi.org/10.5194/nhess-21-1473-2021.

Zhang H., Zheng Y., Wang X.C., Wang Y., Dzakpasu M., 2021. Characterization and biogeochemical implications of dissolved organic matter in aquatic environments. Journal of Environmental Management, 294, 113041. https://doi.org/10.1016/j.jenvman.2021.113041.

Zhang D., Meng F., Wang Y., Zhang L., Xue H., Liang Z., Zhang J., 2023. Seasonal and Spatial Variations in the Optical Characteristics of Dissolved Organic Matter in the Huma River Basin, China. Water, 15(8), 1579. https://doi.org/10.3390/w15081579.

Zheng S., Feng F., Liu D., Qian F., Xie X., Yu H., Song Y, 2026. Hydrological Seasonality Drives DOM-Bacteria Interactions in the Rushan River Basin. Microorganisms, 14(1), 110. https://doi.org/10.3390/microorganisms14010110.

Zhuang W.E., Chen W., Cheng Q., Yang L., 2021. Assessing the priming effect of dissolved organic matter from typical sources using fluorescence EEMs-PARAFAC. Chemosphere 264, 128600. https://doi.org/10.1016/j.chemosphere.2020.128600.

*Table S1*. Meteorological, hydrological, and physico-chemical parameters, as well as nutrient and dissolved organic carbon (DOC) concentrations, in surface waters at the different stations sampled during the dry (March) and wet (July) periods in 2019 along the main channel of the Red River, spanning from the upstream region (UpR; St1-10) to the Red River Delta (RRD; St11-34)

| Station | Precip (mm) | Discharge ($m^3$ $s^{-1}$) | Temp (°C) | EC (µS $cm^{-1}$) | pH | DO (mg $L^{-1}$) | $PO_4^{3-}$ (mg P $L^{-1}$) | $NO_3^-$ (mg N $L^{-1}$) | $NH_4^+$ (mg N $L^{-1}$) | DOC (mg C $L^{-1}$) |
|---|---|---|---|---|---|---|---|---|---|---|
| **Dry season** | | | | | | | | | | |
| St 1 | 3.8 | 1690 | 16 | 353 | 7.56 | 7.44 | *na* | 0.95 | 0.171 | 2.58 |
| St 2 | 3.8 | 1690 | 16 | 292 | 7.71 | 7.71 | *na* | 1.09 | 0.223 | 1.49 |
| St 3 | 3.8 | 1690 | 20 | 6 | 7.61 | 7.89 | *na* | 1.28 | 0.062 | 1.58 |
| St 4 | 3.8 | 1690 | 19 | 5 | 7.55 | 7.60 | *na* | 0.89 | 0.093 | 1.38 |
| St 5 | 2.3 | 1690 | 18 | 237 | 7.50 | 8.26 | *na* | 0.93 | 0.145 | *na* |
| St 6 | 2.3 | 1640 | 14 | 256 | 8.21 | 8.03 | *na* | 1.02 | 0.038 | 2.15 |
| St 7 | 0.9 | 1640 | 17 | 254 | 8.22 | 8.04 | *na* | 0.80 | 0.089 | 3.95 |
| St 8 | 0.9 | 1110 | 18 | 220 | 7.94 | 7.49 | *na* | 1.00 | 0.067 | 1.48 |
| St 9 | 0.9 | 1110 | 18 | *na* | *na* | *na* | *na* | 0.74 | 0.087 | 1.34 |
| St 10 | 0.9 | 1110 | 18 | *na* | *na* | *na* | *na* | 0.80 | 0.100 | *na* |
| St 11 | 0.7 | 1110 | 19 | *na* | *na* | *na* | *na* | 0.89 | 1.597 | *na* |
| St 12 | 0.7 | 1110 | 20 | *na* | *na* | *na* | *na* | 0.93 | 0.060 | *na* |
| St 13 | 0.7 | 1110 | 20 | *na* | *na* | *na* | *na* | 0.34 | 4.897 | *na* |
| St 14 | 0.7 | 1110 | 21 | *na* | *na* | *na* | *na* | 0.56 | 0.523 | *na* |
| St 15 | 0.7 | 1110 | 19 | *na* | *na* | *na* | *na* | 0.60 | 0.555 | *na* |
| St 16 | 1.5 | 1510 | 19 | *na* | *na* | *na* | *na* | 0.62 | 0.023 | 1.41 |
| St 17 | 1.5 | 1510 | 18 | *na* | *na* | *na* | *na* | 1.33 | 0.521 | 1.15 |
| St 18 | 1.5 | 1510 | 18 | 198 | 7.96 | *na* | 0.118 | 0.52 | 0.050 | 1.29 |
| St 19 | 1.5 | 1510 | 16 | 242 | 8.45 | *na* | 1.360 | 0.50 | 0.079 | 1.34 |
| St 20 | 1.5 | 1510 | 16 | 271 | 8.30 | *na* | 0.765 | 0.48 | 0.083 | 1.23 |
| St 21 | 1.3 | 1420 | 18 | 229 | 8.15 | *na* | 0.098 | 0.95 | 0.128 | *na* |
| St 22 | 1.3 | 1420 | 19 | 258 | 8.07 | *na* | 0.124 | 0.79 | 0.725 | *na* |
| St 23 | 1.2 | 1420 | 19 | 272 | 8.01 | *na* | 0.089 | 0.57 | 1.155 | *na* |
| St 24 | 1.2 | 1420 | 18 | 218 | 7.80 | *na* | 0.043 | 0.64 | 0.197 | 1.33 |
| St 25 | 1.2 | 1420 | 20 | 245 | 8.26 | *na* | 0.053 | 0.62 | 0.276 | 1.11 |
| St 26 | 1.2 | 1420 | 18 | 200 | 7.98 | *na* | 0.064 | 0.59 | 0.208 | 2.31 |
| St 27 | 1.2 | 1420 | 18 | 216 | 8.21 | *na* | 0.048 | 0.64 | 0.207 | 1.28 |
| St 28 | 0.8 | 1420 | 19 | 212 | 8.15 | *na* | 0.022 | 0.70 | 0.024 | 1.41 |
| St 29 | 0.8 | 1420 | 19 | 231 | 8.06 | *na* | 0.048 | 1.24 | 0.067 | 1.78 |
| St 30 | 0.6 | 1310 | 20 | 205 | 7.96 | *na* | 0.044 | 0.91 | 0.034 | 1.42 |
| St 31 | 0.6 | 1310 | 20 | 210 | 7.92 | *na* | 0.043 | 0.86 | 0.031 | 1.71 |
| St 32 | 0.6 | 1310 | 20 | 534 | 7.96 | *na* | 0.089 | 1.26 | 0.043 | 0.98 |
| St 33 | 0.6 | 1310 | 19 | 1028 | 7.85 | *na* | 0.047 | 0.89 | 0.052 | *na* |
| St 34 | 0.6 | 1310 | 19 | 5330 | 7.89 | *na* | 0.029 | 0.94 | 0.066 | *na* |
| **Wet season** | | | | | | | | | | |
| St 1 | 12.9 | 2480 | 25 | 168 | 7.79 | 7.21 | 0.154 | 0.54 | 0.063 | 2.20 |
| St 2 | 12.9 | 2480 | 27 | 331 | 7.86 | 6.14 | 0.136 | 1.11 | 0.547 | 1.22 |
| St 3 | 5.8 | 2690 | 29 | 181 | 7.73 | 6.79 | 0.099 | 0.84 | 0.022 | 1.00 |
| St 4 | 5.8 | 2690 | 29 | 155 | 7.52 | 6.79 | 0.304 | 0.54 | 0.052 | *na* |
| St 5 | 17.5 | 2690 | 29 | 141 | 7.64 | 6.31 | 0.161 | 0.78 | 0.137 | 1.22 |
| St 6 | 17.5 | 2690 | 28 | 277 | 7.52 | 5.45 | 0.123 | 0.81 | 0.015 | 1.34 |
| St 7 | 10.4 | 2480 | 28 | 226 | 7.42 | 6.02 | 0.105 | 0.80 | 0.075 | 1.34 |
| St 8 | 10.4 | 2480 | 28 | 217 | 7.39 | 6.68 | 0.228 | 0.81 | 0.044 | *na* |
| St 9 | 8.4 | 2640 | 25 | 241 | 7.90 | 5.50 | 0.045 | 0.75 | 0.063 | 1.30 |
| St 10 | 8.4 | 2640 | 26 | 256 | 7.60 | 4.56 | 0.046 | 0.48 | 0.389 | *na* |
| St 11 | 7.3 | 2640 | 26 | 228 | 7.95 | 6.90 | *na* | 0.79 | 0.046 | 0.94 |
| St 12 | 7.3 | 2640 | 27 | 261 | 7.93 | 5.10 | *na* | 0.93 | 0.457 | 0.91 |

| Station | Precip (mm) | Discharge ($m^3 s^{-1}$) | Temp (°C) | EC ($\mu S\ cm^{-1}$) | pH | DO ($mg\ L^{-1}$) | $PO_4^{3-}$ ($mg\ P\ L^{-1}$) | $NO_3^-$ ($mg\ N\ L^{-1}$) | $NH_4^+$ ($mg\ N\ L^{-1}$) | DOC ($mg\ C\ L^{-1}$) |
|---|---|---|---|---|---|---|---|---|---|---|
| St 13 | 10.1 | 2530 | 28 | 323 | 7.47 | 4.08 | 0.261 | 0.43 | 2.373 | *na* |
| St 14 | 10.1 | 2530 | 28 | 255 | 7.86 | 6.20 | 0.010 | 0.60 | 0.172 | 1.15 |
| St 15 | 10.1 | 2530 | 29 | 248 | 7.93 | 6.22 | *na* | 0.59 | 0.087 | 0.95 |
| St 16 | 10.1 | 2530 | 28 | 243 | 7.90 | 6.59 | *na* | 0.54 | 0.068 | 0.88 |
| St 17 | 10.1 | 2530 | 29 | 250 | 7.88 | 5.16 | *na* | 0.54 | 0.290 | 1.00 |
| St 18 | 10.1 | 2530 | 29 | 224 | 7.88 | 6.15 | 0.102 | 0.71 | 0.285 | 1.16 |
| St 19 | 10.1 | 2530 | 27 | 222 | 7.85 | 6.01 | 0.107 | 0.69 | 0.257 | 1.16 |
| St 20 | 5.2 | 2950 | 27 | 221 | 7.86 | 6.50 | 0.079 | 0.69 | 0.218 | 1.31 |
| St 21 | 5.1 | 2950 | 28 | 215 | 7.82 | 6.51 | 0.092 | 0.79 | 0.192 | 1.23 |
| St 22 | 5.1 | 2950 | 29 | 214 | 7.71 | 6.25 | 0.091 | 0.66 | 0.177 | 1.37 |
| St 23 | 4.6 | 2950 | 28 | 246 | 7.74 | 5.90 | 0.086 | 0.82 | 0.135 | 1.12 |
| St 24 | 4.6 | 2950 | 27 | 236 | 7.64 | 5.55 | 0.065 | 0.87 | 0.141 | 1.29 |
| St 25 | 4.2 | 3160 | 27 | 243 | 7.69 | 5.24 | 0.097 | 0.80 | 0.137 | 1.20 |
| St 26 | 4.2 | 3160 | 29 | 222 | 7.71 | 5.90 | 0.093 | 0.85 | 0.146 | 1.28 |
| St 27 | 4.2 | 3160 | 29 | 233 | 7.91 | 7.35 | 0.079 | 0.84 | 0.117 | 1.29 |
| St 28 | 3.5 | 3160 | 29 | 235 | 7.72 | 6.19 | 0.104 | 0.82 | 0.113 | 1.12 |
| St 29 | 3.5 | 3160 | 29 | 236 | 7.59 | 6.30 | 0.084 | 0.88 | 0.148 | 1.26 |
| St 30 | 3.5 | 3160 | 29 | 240 | 7.81 | 6.70 | 0.075 | 0.77 | 0.077 | 1.14 |
| St 31 | 4.0 | 3160 | 29 | 270 | 7.67 | 6.52 | 0.067 | 0.80 | 0.082 | 1.13 |
| St 32 | 4.0 | 3160 | 29 | 264 | 7.57 | 4.42 | 0.059 | 0.79 | 0.085 | 1.19 |
| St 33 | 4.0 | 3160 | 28 | 259 | 7.73 | 5.45 | 0.131 | 0.74 | 0.064 | 1.19 |
| St 34 | 4.0 | 3160 | 28 | 452 | 7.44 | 4.92 | 0.097 | 0.78 | 0.029 | 1.06 |

*Note*: Precip: precipitation; Temp: water temperature; EC: electrical conductivity; DO: dissolved oxygen; $PO_4^{3-}$: phosphates; $NO_3^-$: nitrates; $NH_4^+$: ammonium; DOC: dissolved organic carbon.
*na*: data not available; Note: some samples were lost during transport, storage, or analysis

*Table S2.* Parameters of chromophoric and fluorescent dissolved organic matter (CDOM and FDOM) in surface waters at the different stations sampled during the dry (March) and wet (July) period in 2019 along the main channel of the Red River, spanning from the upstream region (UpR; St1-10) to the Red River Delta (RRD; St11-34)

| | CDOM | | | | | | FDOM | | | | | |
|---|---|---|---|---|---|---|---|---|---|---|---|---|
| **Station** | **a(254) ($m^{-1}$)** | **a(350) ($m^{-1}$)** | **$E_2/E_3$** | **$SUVA_{254}$ ($mg\ C\ L\ m^{-1}$)** | **$S_{275-295}$ ($nm^{-1}$)** | **$S_R$** | **C1 (QSU)** | **C2 (QSU)** | **C3 (QSU)** | **FI** | **BIX** | **HIX** |
| **Dry period** | | | | | | | | | | | | |
| St 1 | 6.90 | 2.36 | 3.59 | 2.68 | 0.0100 | 1.17 | 34.1 | 58.5 | 26.6 | 0.75 | 0.10 | 1.59 |
| St 2 | 4.64 | 1.65 | 3.58 | 3.10 | 0.0121 | 1.04 | *na* | *na* | *na* | 0.67 | 0.09 | 1.61 |
| St 3 | 7.77 | 2.45 | 4.07 | 4.92 | 0.0123 | 1.00 | 112.1 | 257.6 | 93.9 | 0.92 | 0.09 | 1.95 |
| St 4 | 5.55 | 1.65 | 4.65 | 4.02 | 0.0126 | 0.89 | 43.8 | 112.1 | 28.4 | 0.84 | 0.04 | 1.60 |
| St 5 | *na* | *na* | *na* | *na* | *na* | *na* | *na* | *na* | *na* | *na* | *na* | *na* |
| St 6 | 9.38 | 3.18 | 3.87 | 4.37 | 0.0112 | 0.80 | 102.0 | 68.4 | 69.1 | 1.10 | 0.07 | 5.88 |
| St 7 | 13.02 | 4.29 | 4.04 | 3.30 | 0.0122 | 0.74 | 146.5 | 79.5 | 102.8 | 1.14 | 0.07 | 6.76 |
| St 8 | 6.60 | 1.88 | 4.65 | 4.45 | 0.0130 | 1.02 | 100.6 | 199.2 | 69.9 | 0.73 | 0.07 | 2.16 |
| St 9 | 7.32 | 2.11 | 4.58 | 5.47 | 0.0135 | 1.07 | 52.2 | 65.8 | 34.9 | 0.74 | 0.05 | 3.30 |
| St 10 | *na* | *na* | *na* | *na* | *na* | *na* | *na* | *na* | *na* | *na* | *na* | *na* |
| St 11 | *na* | *na* | *na* | *na* | *na* | *na* | *na* | *na* | *na* | *na* | *na* | *na* |
| St 12 | *na* | *na* | *na* | *na* | *na* | *na* | *na* | *na* | *na* | *na* | *na* | *na* |
| St 13 | *na* | *na* | *na* | *na* | *na* | *na* | *na* | *na* | *na* | *na* | *na* | *na* |
| St 14 | *na* | *na* | *na* | *na* | *na* | *na* | *na* | *na* | *na* | *na* | *na* | *na* |
| St 15 | *na* | *na* | *na* | *na* | *na* | *na* | *na* | *na* | *na* | *na* | *na* | *na* |
| St 16 | 4.92 | 1.24 | 5.36 | 3.48 | 0.0152 | 1.23 | 31.6 | 64.0 | 19.9 | 0.67 | 0.09 | 0.56 |
| St 17 | 4.93 | 1.35 | 4.75 | 4.30 | 0.0147 | 1.34 | 54.4 | 192.6 | 38.4 | 0.92 | 0.06 | 1.30 |
| St 18 | 4.82 | 1.20 | 5.45 | 3.73 | 0.0145 | 1.08 | 34.0 | 60.3 | 20.4 | 0.71 | 0.02 | 2.32 |

| | CDOM | | | | | | FDOM | | | | | |
|---|---|---|---|---|---|---|---|---|---|---|---|---|
| **Station** | **a(254) ($m^{-1}$)** | **a(350) ($m^{-1}$)** | **$E_2/E_3$** | **$SUVA_{254}$ (mg C L $m^{-1}$)** | **$S_{275-295}$ ($nm^{-1}$)** | **$S_R$** | **C1 (QSU)** | **C2 (QSU)** | **C3 (QSU)** | **FI** | **BIX** | **HIX** |
| St 19 | 6.76 | 1.89 | 4.67 | 5.05 | 0.0144 | 1.22 | 73.0 | 185.5 | 52.4 | 0.94 | 0.09 | 1.71 |
| St 20 | 5.85 | 1.49 | 5.39 | 4.77 | 0.0149 | 1.06 | 74.1 | 136.7 | 55.0 | 0.94 | 0.10 | 0.87 |
| St 21 | *na* | *na* | *na* | *na* | *na* | *na* | *na* | *na* | *na* | *na* | *na* | *na* |
| St 22 | *na* | *na* | *na* | *na* | *na* | *na* | *na* | *na* | *na* | *na* | *na* | *na* |
| St 23 | *na* | *na* | *na* | *na* | *na* | *na* | *na* | *na* | *na* | *na* | *na* | *na* |
| St 24 | 5.88 | 1.62 | 4.84 | 4.42 | 0.0138 | 1.15 | 35.8 | 110.1 | 22.6 | 0.71 | 0.04 | 1.39 |
| St 25 | 6.18 | 1.79 | 4.44 | 5.54 | 0.0138 | 1.25 | 71.3 | 189.9 | 52.6 | 0.71 | 0.09 | 1.44 |
| St 26 | 13.09 | 3.31 | 5.23 | 5.67 | 0.0150 | 1.07 | 94.1 | 55.1 | 71.0 | 0.69 | 0.10 | 7.59 |
| St 27 | 6.38 | 1.78 | 4.82 | 4.98 | 0.0136 | 1.07 | 44.5 | 102.8 | 30.2 | 0.68 | 0.16 | 0.33 |
| St 28 | 5.91 | 1.76 | 4.50 | 4.19 | 0.0132 | 1.12 | 74.8 | 127.0 | 54.8 | 0.69 | 0.12 | 1.05 |
| St 29 | 6.16 | 1.68 | 4.89 | 3.46 | 0.0138 | 1.11 | 76.5 | 235.1 | 52.1 | 0.67 | 0.08 | 1.41 |
| St 30 | 6.58 | 1.83 | 4.73 | 4.65 | 0.0136 | 1.13 | 42.6 | 51.4 | 29.2 | 0.67 | 0.12 | 0.57 |
| St 31 | 7.02 | 2.11 | 4.25 | 4.12 | 0.0132 | 1.24 | 41.6 | 58.7 | 27.7 | 0.68 | 0.13 | 1.30 |
| St 32 | 3.61 | 0.79 | 5.57 | 3.70 | 0.0166 | 1.05 | 50.6 | 64.4 | 34.2 | 0.65 | 0.09 | 2.21 |
| St 33 | 4.08 | 0.92 | 6.15 | 4.55 | 0.0173 | 1.27 | 56.6 | 137.9 | 39.3 | 0.61 | 0.09 | 1.74 |
| St 34 | *na* | *na* | *na* | *na* | *na* | *na* | *na* | *na* | *na* | *na* | *na* | *na* |
| **Wet period** | | | | | | | | | | | | |
| St 1 | 23.47 | 8.06 | 3.58 | 10.67 | 0.0110 | 0.91 | 214.7 | 374.0 | 99.1 | 0.56 | 0.05 | 2.11 |
| St 2 | 12.64 | 5.33 | 2.76 | 10.36 | 0.0093 | 1.33 | 124.7 | 499.2 | 76.7 | 0.64 | 0.07 | 1.06 |
| St 3 | 9.78 | 3.55 | 3.28 | 9.78 | 0.0109 | 1.24 | 104.0 | 397.1 | 61.6 | 0.62 | 0.06 | 1.13 |
| St 4 | *na* | *na* | *na* | *na* | *na* | *na* | *na* | *na* | *na* | *na* | *na* | *na* |
| St 5 | 18.92 | 8.77 | 2.45 | 15.51 | 0.0085 | 1.09 | 140.8 | 431.2 | 83.8 | 0.64 | 0.07 | 1.37 |
| St 6 | 19.22 | 9.50 | 2.29 | 14.34 | 0.0079 | 1.27 | 136.3 | 517.3 | 83.0 | 0.63 | 0.06 | 1.11 |
| St 7 | 19.47 | 8.77 | 2.56 | 14.53 | 0.0089 | 1.03 | 150.8 | 518.5 | 95.3 | 0.66 | 0.06 | 1.24 |
| St 8 | *na* | *na* | *na* | *na* | *na* | *na* | *na* | *na* | *na* | *na* | *na* | *na* |
| St 9 | 11.52 | 3.59 | 3.96 | 8.86 | 0.0125 | 1.10 | 141.3 | 471.7 | 88.2 | 0.63 | 0.06 | 1.33 |
| St 10 | *na* | *na* | *na* | *na* | *na* | *na* | *na* | *na* | *na* | *na* | *na* | *na* |
| St 11 | 8.48 | 3.45 | 2.95 | 9.02 | 0.0087 | 1.20 | 82.0 | 466.8 | 56.6 | 0.64 | 0.05 | 0.86 |
| St 12 | 11.75 | 5.32 | 2.52 | 12.91 | 0.0091 | 1.71 | 76.3 | 292.1 | 52.9 | 0.66 | 0.06 | 1.35 |
| St 13 | *na* | *na* | *na* | *na* | *na* | *na* | *na* | *na* | *na* | *na* | *na* | *na* |
| St 14 | 8.51 | 2.67 | 3.99 | 7.40 | 0.0129 | 1.17 | 106.9 | 426.0 | 71.9 | 0.67 | 0.06 | 1.17 |
| St 15 | 8.70 | 3.12 | 3.24 | 9.16 | 0.0111 | 1.36 | 90.8 | 549.4 | 61.3 | 0.65 | 0.06 | 0.76 |
| St 16 | 12.57 | 6.10 | 2.31 | 14.28 | 0.0090 | 1.72 | 92.6 | 435.0 | 62.2 | 0.67 | 0.06 | 0.99 |
| St 17 | 6.75 | 1.98 | 4.25 | 6.75 | 0.0132 | 1.22 | 88.1 | 359.1 | 58.9 | 0.64 | 0.06 | 1.14 |
| St 18 | 15.48 | 6.98 | 2.52 | 13.36 | 0.0091 | 1.35 | 122.3 | 262.5 | 72.8 | 0.63 | 0.06 | 2.13 |
| St 19 | 17.14 | 8.85 | 2.20 | 14.72 | 0.0076 | 1.40 | 122.8 | 554.3 | 75.2 | 0.63 | 0.07 | 0.98 |
| St 20 | 13.74 | 6.08 | 2.52 | 10.52 | 0.0101 | 1.86 | 126.8 | 427.8 | 76.9 | 0.64 | 0.06 | 1.31 |
| St 21 | 11.64 | 4.09 | 3.49 | 9.46 | 0.0110 | 0.98 | 124.4 | 347.4 | 74.7 | 0.63 | 0.06 | 1.55 |
| St 22 | 9.74 | 3.05 | 3.89 | 7.10 | 0.0131 | 1.44 | 126.3 | 392.7 | 74.8 | 0.63 | 0.06 | 1.45 |
| St 23 | 9.70 | 3.69 | 3.19 | 8.65 | 0.0112 | 1.35 | 115.2 | 285.5 | 74.6 | 0.64 | 0.06 | 1.92 |
| St 24 | 9.92 | 3.43 | 3.54 | 7.67 | 0.0117 | 1.22 | 119.5 | 287.5 | 74.8 | 0.64 | 0.06 | 1.85 |
| St 25 | 10.29 | 3.77 | 3.38 | 8.60 | 0.0118 | 1.22 | 119.0 | 284.5 | 75.9 | 0.65 | 0.06 | 2.01 |
| St 26 | 12.60 | 4.81 | 3.11 | 9.82 | 0.0107 | 1.14 | 125.7 | 502.1 | 82.8 | 0.66 | 0.06 | 1.18 |
| St 27 | 11.04 | 4.00 | 3.30 | 8.58 | 0.0110 | 1.11 | 127.6 | 365.7 | 82.8 | 0.65 | 0.06 | 1.62 |
| St 28 | 11.08 | 4.07 | 3.21 | 9.87 | 0.0123 | 1.36 | 122.5 | 368.8 | 79.3 | 0.65 | 0.06 | 1.56 |
| St 29 | 13.30 | 6.48 | 2.29 | 10.59 | 0.0085 | 1.72 | 114.7 | 390.0 | 71.9 | 0.64 | 0.06 | 1.36 |
| St 30 | 8.89 | 2.86 | 3.78 | 7.83 | 0.0125 | 1.39 | 109.5 | 366.3 | 70.7 | 0.63 | 0.06 | 1.39 |
| St 31 | 7.51 | 1.92 | 5.05 | 6.64 | 0.0144 | 1.08 | 101.3 | 417.7 | 66.0 | 0.63 | 0.06 | 1.15 |
| St 32 | 8.52 | 3.11 | 3.23 | 7.19 | 0.0116 | 1.63 | 98.0 | 524.0 | 67.7 | 0.65 | 0.06 | 0.89 |
| St 33 | 9.45 | 3.73 | 2.94 | 7.93 | 0.0109 | 1.63 | 101.6 | 496.5 | 70.4 | 0.66 | 0.06 | 0.98 |
| St 34 | 7.91 | 2.26 | 4.36 | 7.46 | 0.0140 | 1.38 | 106.0 | 532.4 | 70.7 | 0.65 | 0.06 | 0.92 |

*Table S2-Note*: a(254) and a(350): CDOM absorption coefficients at 254 and 350 nm; $E_2/E_3$: a(250)/a(365); $SUVA_{254}$: specific UV absorbance at 254 nm, i.e., a(254)/DOC; $S_{275-295}$: spectral slope coefficient of CDOM absorption between 275 and 295 nm; $S_R$: CDOM slope ratio, i.e., $S_{275-295}/S_{350-400}$; C1, C2 and C3: FDOM components validated by PARAFAC modeling, i.e., humic-like UV-C + UV-A ($\lambda_{Ex1}$, $\lambda_{Ex2}/\lambda_{Em}$: < 240, 340/524 nm), tryptophan-like ($\lambda_{Ex}/\lambda_{Em}$: 270/348 nm) and humic-like UV-C + UV-B ($\lambda_{Ex1}$, $\lambda_{Ex2}/\lambda_{Em}$: 240, 310/440 nm), respectively; FI: fluorescence index, i.e., the ratio of fluorescence intensity at $\lambda_{Em}$ of 450 nm to $\lambda_{Em}$ of 500 nm at $\lambda_{Ex}$ of 370 nm; HIX: humification index, i.e., the integral of the fluorescence intensities between $\lambda_{Em}$ of 435 and 480 nm divided by the integral of the fluorescence intensities between $\lambda_{Em}$ of 300 and 345 nm at $\lambda_{Ex}$ of 255 nm; BIX: biological index, i.e., the fluorescence intensity at $\lambda_{Em}$ of 380 nm divided by the fluorescence intensity at $\lambda_{Em}$ of 430 nm at $\lambda_{Ex}$ of 310 nm. *na*: data not available; Note: some samples were lost during transport, storage, or analysis

*Table S3.* Explained variance of each principal component and variable loadings (correlations between variables and principal components) obtained from the PCA

| | **F1** | **F2** | **F3** | **F4** | **F5** |
|---|---|---|---|---|---|
| Eigenvalue | 6.5 | 2.8 | 1.0 | 0.9 | 0.6 |
| Variance (%) | 50.2 | 21.8 | 7.5 | 6.6 | 4.3 |
| Cumulative (%) | 50.2 | 72.0 | 79.6 | 86.1 | 90.5 |
| **Variable loadings** | | | | | |
| DOC | -0.23 | 0.86 | 0.20 | -0.03 | 0.01 |
| a(254) | 0.87 | 0.36 | 0.15 | 0.12 | -0.21 |
| a(350) | 0.91 | 0.21 | 0.24 | -0.02 | -0.18 |
| $E_2/E_3$ | -0.91 | 0.03 | -0.22 | 0.25 | -0.12 |
| $SUVA_{254}$ | 0.94 | -0.12 | 0.09 | 0.00 | -0.14 |
| $S_{275-295}$ | -0.85 | -0.06 | -0.30 | 0.29 | 0.00 |
| $S_R$ | 0.41 | -0.61 | 0.13 | -0.33 | 0.21 |
| C1 | 0.80 | 0.42 | -0.24 | 0.29 | 0.11 |
| C2 | 0.84 | -0.27 | -0.26 | 0.12 | 0.25 |
| C3 | 0.74 | 0.47 | -0.25 | 0.24 | 0.30 |
| FI | -0.42 | 0.61 | 0.03 | -0.41 | 0.40 |
| BIX | -0.44 | 0.02 | 0.71 | 0.47 | 0.24 |
| HIX | -0.19 | 0.83 | -0.09 | -0.20 | -0.18 |

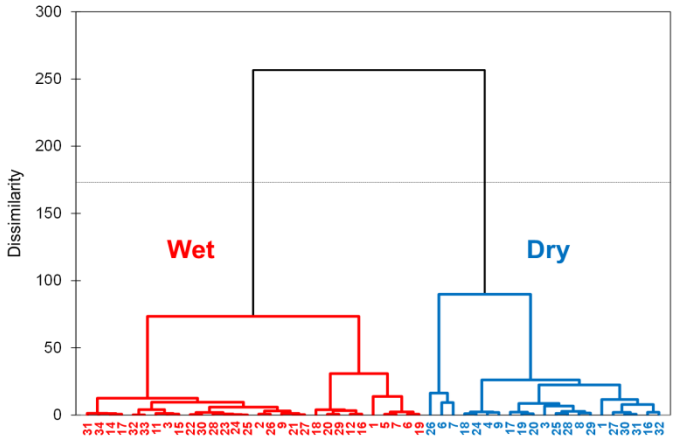


*Figure S1.* Ascending hierarchical classification (AHC) performed on DOC and CDOM and FDOM parameters, i.e., a(254), a(350), $E_2/E_3$, $SUVA_{254}$, $S_{275-295}$, $S_R$, C1, C2, C3, FI, BIX, and HIX, for all available samples (n = 51). Group dissimilarity was assessed using Ward's method based on squared Euclidean distance. Stations sampled during the dry period are shown in blue and those sampled during the wet period in red. Data were centered and standardized beforehand

*Table S4.* Pairwise Pearson correlation matrix showing correlation coefficients (r) of linear relationships between meteorological, hydrological, physico-chemical parameters, nutrients, DOC, and CDOM and FDOM parameters (n = 29-68). Only very highly significant correlations ($p < 0.0001$) are shown in bold (blue for negative correlations and red for positive correlations)

| | **Precip** | **Disch** | **Temp** | **EC** | **pH** | **DO** | **$NO_3^-$** | **$NH_4^+$** | **$PO_4^{3-}$** | **DOC** | **a(254)** | **a(350)** | **$E_2/E_3$** | **$SUVA_{254}$** | **$S_{275-295}$** | **$S_R$** | **C1** | **C2** | **C3** | **FI** | **BIX** |
|---|---|---|---|---|---|---|---|---|---|---|---|---|---|---|---|---|---|---|---|---|---|
| **Disch** | **0.60** | | | | | | | | | | | | | | | | | | | | |
| **Temp** | **0.68** | **0.91** | | | | | | | | | | | | | | | | | | | |
| **EC** | -0.16 | -0.19 | -0.14 | | | | | | | | | | | | | | | | | | |
| **pH** | -0.44 | **-0.54** | **-0.55** | 0.04 | | | | | | | | | | | | | | | | | |
| **DO** | -0.35 | **-0.63** | **-0.66** | -0.41 | 0.29 | | | | | | | | | | | | | | | | |
| **$NO_3^-$** | -0.16 | -0.10 | -0.19 | 0.12 | -0.11 | 0.49 | | | | | | | | | | | | | | | |
| **$NH_4^+$** | -0.07 | -0.19 | -0.07 | -0.04 | -0.09 | -0.42 | -0.32 | | | | | | | | | | | | | | |
| **$PO_4^{3-}$** | -0.04 | -0.15 | -0.26 | -0.08 | 0.36 | 0.07 | -0.35 | 0.03 | | | | | | | | | | | | | |
| **DOC** | -0.23 | -0.36 | -0.49 | -0.08 | 0.19 | 0.56 | 0.09 | -0.14 | -0.01 | | | | | | | | | | | | |
| **a(254)** | **0.74** | **0.50** | **0.53** | -0.25 | -0.31 | -0.13 | -0.20 | 0.08 | -0.10 | 0.14 | | | | | | | | | | | |
| **a(350)** | **0.78** | **0.52** | **0.57** | -0.21 | -0.35 | -0.19 | -0.14 | 0.13 | -0.10 | 0.00 | **0.96** | | | | | | | | | | |
| **$E_2/E_3$** | **-0.69** | **-0.69** | **-0.68** | 0.32 | 0.41 | 0.30 | 0.02 | -0.22 | 0.15 | 0.18 | **-0.72** | **-0.82** | | | | | | | | | |
| **$SUVA_{254}$** | **0.81** | **0.67** | **0.78** | -0.15 | -0.38 | -0.46 | -0.22 | 0.18 | -0.12 | -0.38 | **0.82** | **0.90** | **-0.83** | | | | | | | | |
| **$S_{275-295}$** | **-0.70** | **-0.56** | **-0.55** | 0.37 | 0.37 | 0.08 | 0.01 | -0.19 | 0.16 | 0.07 | **-0.73** | **-0.84** | **0.96** | **-0.79** | | | | | | | |
| **$S_R$** | 0.17 | 0.49 | **0.52** | 0.13 | -0.22 | -0.58 | -0.13 | 0.28 | -0.08 | -0.50 | 0.10 | 0.24 | -0.47 | 0.43 | -0.32 | | | | | | |
| **C1** | **0.60** | **0.64** | **0.60** | -0.19 | -0.30 | -0.03 | -0.08 | 0.01 | -0.09 | 0.13 | **0.83** | **0.73** | **-0.61** | **0.65** | **-0.54** | 0.01 | | | | | |
| **C2** | **0.69** | **0.83** | **0.86** | -0.08 | -0.50 | **-0.62** | -0.11 | 0.09 | -0.14 | -0.43 | **0.55** | **0.60** | **-0.71** | **0.75** | **-0.60** | 0.46 | **0.65** | | | | |
| **C3** | 0.51 | **0.61** | **0.56** | -0.21 | -0.25 | -0.01 | -0.01 | 0.01 | -0.06 | 0.16 | **0.73** | **0.64** | **-0.58** | **0.58** | -0.50 | 0.01 | **0.95** | **0.64** | | | |
| **FI** | -0.38 | -0.47 | **-0.64** | -0.17 | 0.47 | 0.59 | 0.17 | -0.02 | **0.84** | **0.55** | -0.24 | -0.27 | 0.28 | -0.46 | 0.21 | -0.43 | -0.18 | -0.48 | -0.04 | | |
| **BIX** | -0.35 | -0.51 | -0.46 | 0.15 | 0.42 | 0.37 | 0.11 | -0.06 | 0.10 | 0.21 | -0.27 | -0.28 | 0.34 | -0.37 | 0.31 | -0.18 | -0.35 | -0.45 | -0.30 | 0.12 | |
| **HIX** | -0.24 | -0.28 | -0.38 | -0.02 | 0.27 | 0.53 | 0.04 | -0.04 | -0.02 | **0.71** | 0.12 | -0.01 | 0.19 | -0.24 | 0.14 | -0.43 | 0.14 | -0.42 | 0.21 | **0.52** | -0.04 |

Disch: discharge; other variables are defined in Tables S1 and S2

*Table S5.* Results of the Mann-Whitney rank-sum tests used to compare DOM (DOC, CDOM, FDOM) and environmental variables between hydrological periods (dry *vs*. wet) and spatial sectors (UpR *vs*. RDD). For each comparison, the Mann-Whitney statistic (U), standardized test statistic (Z or normalized U), p-value, total sample size (N), and effect size ($r = |Z| / \sqrt{N}$) are provided; p-values in bold denote statistically significant differences between groups ($p < 0.05$)

| | **U** | **Z** | **p** | **N** | **r** |
|---|---|---|---|---|---|
| **Dry *vs*. wet** | | | | | |
| Precip | 12 | -6.95 | < **0.0001** | 68 | 0.84 |
| Discharge | 0 | -7.12 | < **0.0001** | 68 | 0.86 |
| Temp | 0 | -7.16 | < **0.0001** | 68 | 0.87 |
| EC | 425 | 0.00 | 1.000 | 59 | 0.00 |
| $PO_4^{3-}$ | 160 | -1.96 | 0.050 | 46 | 0.29 |
| $NO_3^-$ | 710 | 1.61 | 0.107 | 68 | 0.20 |
| $NH_4^+$ | 574 | -0.04 | 0.966 | 68 | 0.01 |
| DOC | 544 | 3.95 | < **0.0001** | 52 | 0.55 |
| a(254) | 58 | -5.15 | < **0.0001** | 53 | 0.71 |
| a(350) | 44 | -5.40 | < **0.0001** | 53 | 0.74 |
| $E_2/E_3$ | 654 | 5.49 | < **0.0001** | 53 | 0.75 |
| $SUVA_{254}$ | 0 | -6.19 | < **0.0001** | 53 | 0.85 |
| $S_{275-295}$ | 607 | 4.70 | < **0.0001** | 53 | 0.65 |
| $S_R$ | 148 | -3.54 | **0.000** | 53 | 0.49 |
| C1 | 60 | -5.00 | < **0.0001** | 52 | 0.69 |
| C2 | 0 | -6.11 | < **0.0001** | 52 | 0.85 |
| C3 | 87 | -4.50 | < **0.0001** | 52 | 0.62 |
| FI | 651 | 5.49 | < **0.0001** | 53 | 0.75 |
| BIX | 561 | 3.92 | < **0.0001** | 53 | 0.54 |
| HIX | 460 | 2.06 | **0.040** | 53 | 0.28 |
| **UpR *vs*. RDD** | | | | | |
| DOC dry | 90 | 2.32 | **0.020** | 22 | 0.49 |
| DOC wet | 125 | 2.16 | **0.030** | 30 | 0.39 |
| a(350) dry | 97 | 2.36 | **0.016** | 23 | 0.49 |

| | U | Z | p | N | r |
|---|---|---|---|---|---|
| a(350) wet | 127 | 2.28 | **0.021** | 30 | 0.42 |
| C1 dry | 74 | 1.56 | 0.142 | 22 | 0.33 |
| C1 wet | 142 | 3.02 | **0.001** | 30 | 0.55 |
| C2 dry | 57 | 0.32 | 0.783 | 22 | 0.07 |
| C2 wet | 110 | 1.45 | 0.158 | 30 | 0.26 |
| C3 dry | 72 | 1.37 | 0.185 | 22 | 0.29 |
| C3 wet | 138 | 2.82 | **0.003** | 30 | 0.51 |
| $S_{275-295}$ dry | 2 | -3.74 | **< 0.0001** | 23 | 0.78 |
| $S_{275-295}$ wet | 48 | -1.59 | 0.118 | 30 | 0.29 |
| C2/C1 dry | 34 | -1.30 | 0.210 | 22 | 0.28 |
| C2/C1 wet | 42 | -0.74 | 0.490 | 22 | 0.16 |
| C2/C3 dry | 32 | -1.45 | 0.162 | 22 | 0.31 |
| C2/C3 wet | 52 | -0.04 | 1.000 | 22 | 0.01 |
| %C2 dry | 34 | -1.30 | 0.210 | 22 | 0.28 |
| %C2 wet | 46 | -0.46 | 0.680 | 22 | 0.10 |

Variables are defined in Tables S1 and S2